



Institutionen för vattenbyggnad
Chalmers Tekniska Högskola
Department of Hydraulics
Chalmers University of Technology

On the Wave Climate of the Southern Baltic

Nils Mårtensson
Lars Bergdahl

Report
Series A:15
ISSN 0348-1050

Göteborg 1987

Address: Department of Hydraulics
Chalmers University of Technology
S-412 96 Göteborg, Sweden
Telephone: 031/810100

SUMMARY

The wave climate of the southern Baltic is rather mild, with a mean energy flux of 5-6 kW/m. This is to be compared with the average in the North Sea, which is 20-30 kW/m. The ratio of the ten percentile of the mean energy flux to the mean over the measuring period, is lower for the Baltic than for the North Sea (3 compared to 5). This also indicates the mildness of waves of the Southern Baltic.

A comparison is done between wave data from two measuring sites in the southern Baltic. The comparison shows that south of Öland, at "Ölands södra grund", there is more energy in the waves than at Hoburg at the south of Gotland. In fact there is 20% more energy at "Ölands södra grund". The measuring site at Hoburg is, however, somewhat affected by the island of Gotland. It would, therefore, be of great interest to choose another measuring site at Gotland. Presumably "Hoburgs bankar" would give a higher mean wave energy.

Using wind statistics it is noticed that the wind energy flux is 20% higher at ØSG than at Hoburg. This indicates (regarding the fetches) that the wind climate is stronger at ØSG. Although the meteorologists at SMHI have their doubts about the validity of the wind statistics, it is concluded that the 20% difference has some significance.

A more thorough evaluation is performed on the wave climate of ØSG. This evaluation includes mean average spectra and scatter diagrams for the eight cardinal wind directions. The energy flux versus its probability of occurrence is also presented.

The wave data used in this study is taken from two different periods. In the comparison between Hoburg and ØSG, the data is taken from the latter half year of 1981. In the analysis of ØSG the data is taken from the period October 1978 to November 1980.

PREFACE

This work has been performed as a part of the Swedish wave energy research program and was first published 1983. The work has been supported by the Swedish Energy Research Commission (EFN).

For the purpose of being a partial fulfillment of the requirements for the degree of Licentiate of Engineering, the first edition has been somewhat revised.

Lars Bergdahl has participated in the preparation of the report in his capacity as tutor to Nils Mårtensson.

Göteborg, April 1987

Nils Mårtensson

Lars Bergdahl

LIST OF CONTENTS

	Page
SUMMARY	i
PREFACE	ii
LIST OF CONTENTS	iii
1 THE SWEDISH WAVE MEASURING PROGRAMME	1
2 MEASURING DEVICES AND ANALYSIS	3
3 WAVE CLIMATE AT ÖLANDS SÖDRA GRUND (OSG)	8
3.1 General aspects	8
3.1.1 Monthly averaged energy fluxes	8
3.1.2 H_s - T_z scatterdiagram	11
3.1.3 H_s - T_z relation	25
3.2 Energy flux	26
3.2.1 Wave power duration	26
3.2.2 P- H_s - T_z relation	27
3.2.3 Accumulated wave energy distribution	29
4 GEOGRAPHICAL DISTRIBUTION OF WAVE ENERGY	30
4.1 Introduction	30
4.2 Primary wave generation aspects	31
4.2.1 Wind climate	31
4.2.2 Efficient fetches	34
4.3 Wave climate	37
4.3.1 General aspects	37
4.3.2 Extreme month	40
4.3.3 Wave parameters	42
4.4 Curvature of isobars	48
4.4.1 Theoretic wind speeds	49
4.4.2 Isobaric fetch limitations	50
4.5 Shoaling effects at Ölands södra grund	52
LIST OF ABBREVIATIONS AND SYMBOLS	55
LIST OF FIGURES	58
REFERENCES	61
BIBLIOGRAPHY	62

1 THE SWEDISH WAVE MEASURING PROGRAMME

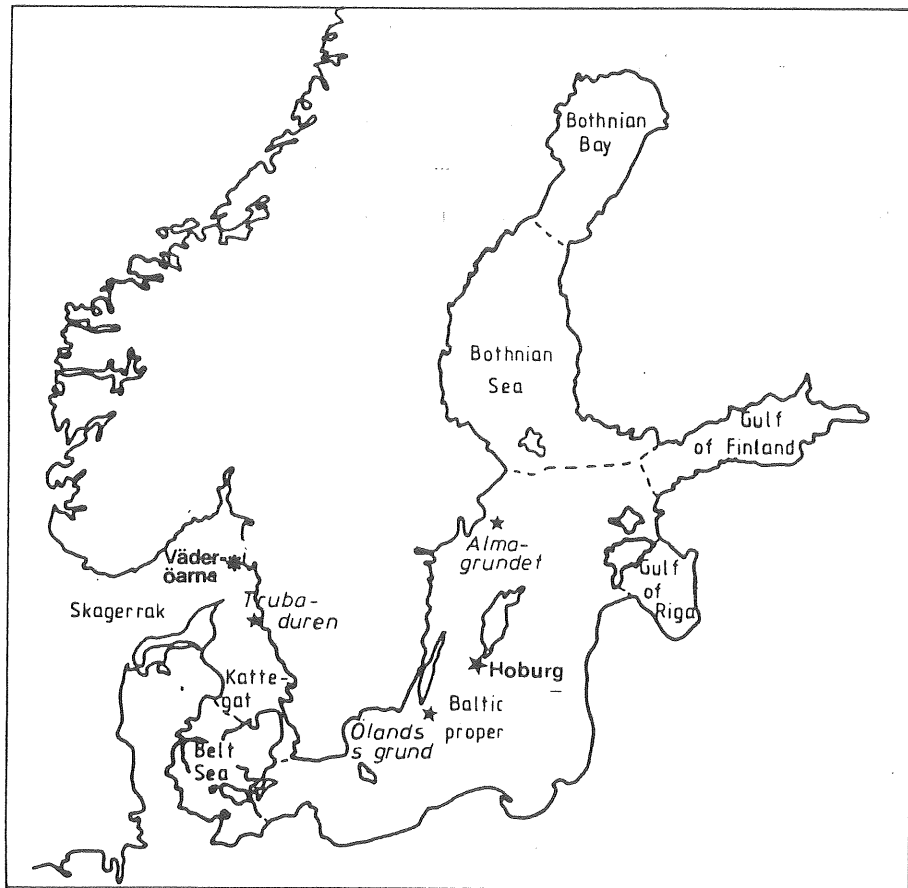


Figure 1.1 Wave measurements are carried out (with fixed devices at the three lighthouses Almagrundet, Ölands södra grund and Trubaduren, and with a mobile device at Hoburg and Väderöarna.

In order to evaluate the amount of wave energy in Swedish waters, SMHI (Swedish Meteorological and Hydrological Institute, Norrköping) has started wave measurements at three fixed automatic measuring stations; Almagrundet and Ölands södra grund in the Baltic Sea and Trubaduren in the Kattegat. As a complement to these fixed stations, equipped with inverted echo-sounders (see Chap. 2), a wave-rider buoy has been deployed at Väderöarna in the Skagerrak and at Hoburg in the Baltic.

The wave measurements were started in the autumn of 1978 and is still going on. They are financed by the Swedish Energy Research Commission (EFN) and is part of the evaluation of the technical and economical possibilities for wave power plants in Swedish coastal waters.

Data from the different stations are received for the following periods:

Almagrundet	Oct. 1978 -
Ølands södra grund	Oct. 1978 -
Trubaduren	Oct. 1978 -
Väderöarna	Apr. 1980 - Jan. 1981
Hoburg	Jun. 1981 -

2 MEASURING DEVICES AND ANALYSIS

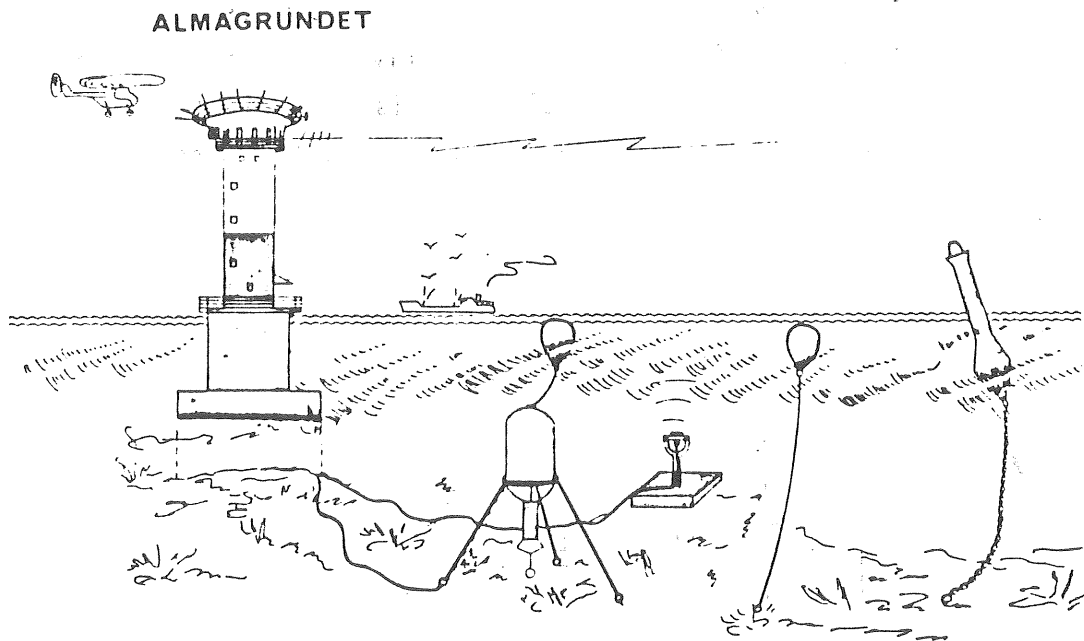


Figure 2.1 The inverted echo-sounder is placed on the sea bed at a depth of 25 m and about 100 m from the light-house. (From Mattisson (1980))

In Mattisson (1980) the measuring devices and analyses are presented as follows.

The fixed wave measuring systems are located at three lighthouses, where SMHI has automatic stations for collection of meteorological and oceanographical data. The mobile station, usually, only measures wave properties and no other data.

The wave measurements are performed with two different devices; inverted echo-sounders at the fixed stations and a wave-rider buoy at the mobile station.

The inverted echo-sounders are placed at a depth of 20-25 metres. A microcomputer, which is the central unit in the automatic station, samples the wave record and computes the wave spectra and some other characteristic wave data. The data are then transmitted to SMHI once an hour by an automatic transmission system. In the mobile system the water level variation is tape recorded and subsequently taken to SMHI for evaluation.

In figure 2.1 the measuring device second from the left is an inverted echo-sounder. Principally, it works by sending out pressure pulses from the sea-bed. These pulses are reflected at the sea surface and are then recorded on the sea-bed by the device. As the velocity of sound is nearly constant in water, if there are no dispersed air-bubbles, it is possible to calculate the distance which the pulse has travelled very precisely.

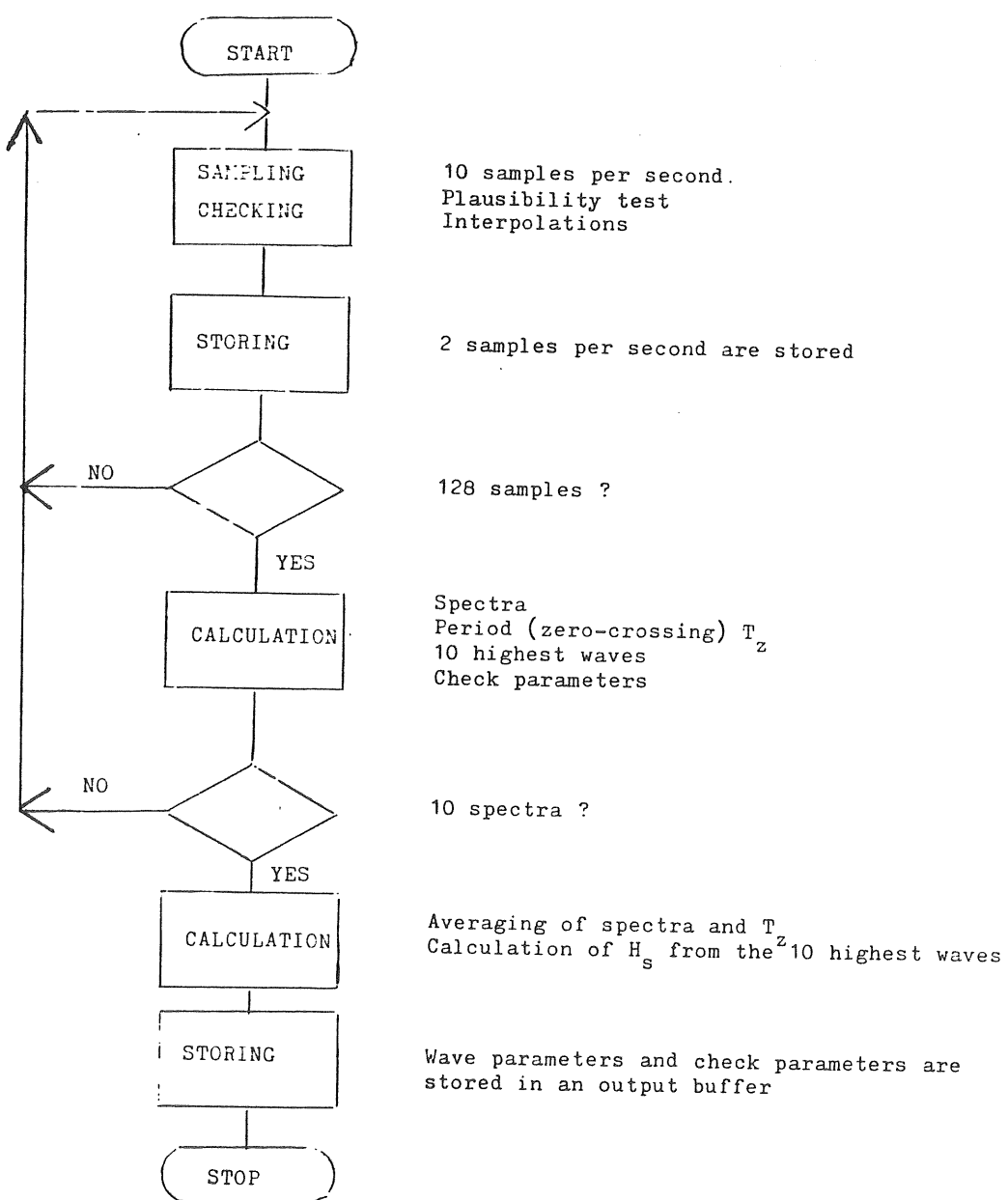


Figure 2.2 Generalized flow chart of the microprocessor program. (Mattisson (1980))

With a frequency of 13 Hz the transceiver send out short pulses (pulse duration $56 \cdot 10^{-6}$ s) of 710 kHz and the time difference between the output and the input pulse (the reflected) is measured and transformed to an analog voltage which is proportional to the distance between the transceiver and the water surface (AM, Amplitude modulated). The variation in this voltage gives the wave record, that is to say, the water level as a function of time.

The automatic measuring stations, at which the wave gauges are placed, are equipped with microprocessors of the programmable type, manufactured by ASEA, Sweden. The stations are integral parts of SMHI's system for the automatic data acquisition of meteorological and oceanographical data.

The wave record, which is available as a varying voltage at the transceiver, is sampled with a frequency of 10 Hz during approximately 11 minutes each hour. During sampling, the wave record is filtered through a low-pass filter with a 3 dB cut-off frequency at 0.67 Hz.

A programme has been devised for the automatic stations, which performs a spectral analysis of the wave record with "Fast Fourier Transform" (FFT) technique (Brigham (1974)).

Before proceeding with the spectral analysis the digital wave data passes through a plausibility test. In this test the difference, H , in water level between two successive samples is not allowed to exceed a certain value h . This value, h , is automatically adjusted to the existing sea conditions. The adjustment is based on knowledge of the wave period and how steep the wave can be. In this way, false measurements caused by outer interference with the natural conditions, are eliminated. (This implies that breaking waves or peak waves and other higher order phenomena will be discarded).

Spectral analysis is done in ten steps with the FFT technique. Each step involves the analysis of a digital wave record of 128 values from a time period of 64 seconds. When the 10 spectral analyses have been made on a total of 1280 checked values, then

the final result is computed as the average of the 10 energy spectra. (It may seem too strange only to use 128 values, but the averaging procedure will give a good spectral estimate, in fact better than a uncritical use of one 1280 sample.)

During the whole measuring sequence the number of "zero down-crossings" are counted and the ten largest waves registered. From these data the mean period T_z (zero crossing period) and the significant waveheight, H_s , are obtained. (Note that these are the parameters referred to as measured.)

The significant wave height is calculated (assuming Rayleigh distributed wave heights) as

$$H_s = H_{10} \left(\frac{1}{2} \ln N/10 \right)^{-\frac{1}{2}} \quad (2.1)$$

where H_{10} is the 10th highest wave and N is the total number of waves.

The data obtained from the wave gauge programme and transmitted to SMHI are as follows (Mattisson (1980)):

a) Wave parameters:

- 30 spectral densities. (These are the discrete frequencies from 5 to 42 over 64 Hz. With the high frequency tail lumped, due to its low energy content.)
- The 5 highest waves.
- Significant wave height, calculated from the 10th highest wave.
- Mean period, calculated from the number of "zero-down-crossings".

b) Check parameters:

- Total number of rejected samples in the observed time series.
- Average height of the rejected samples.
- Standard deviation of rejected samples.
- Number of rejected measuring periods.
- The average value of the calculated mean water levels.
- Standard deviation of mean water level.

Some data about the wave measuring system:

Wave height measuring range: 0-10 m
A/D resolution: 12 bits
Sampling interval: 0.5s (0.1s before data plausibility test)
Duration of sampling: $10 \times 64\text{s} \approx 11 \text{ minutes}$
Total number of samples: 1280 (6400 before data plausibility test)
Number of lags: 38
Frequency interval: 1/64 Hz
Frequency range: $(5/64) - (42/64) = 0.08 - 0.66 \text{ Hz}$
Wave period range: 12.8 - 1.5 s

All information from the measuring sites is stored in a computer at SMHI in Norrköping, and is available for use whenever needed.

3 WAVE CLIMATE AT ÖLANDS SÖDRA GRUND (ÖSG)

3.1 General aspects

3.1.1 Monthly averaged energy fluxes

Wave measurements at Ölands södra grund, ÖSG (a shoal south of the island of Öland), started in October 1978 and are still going on.

Wave data measured at ÖSG, were obtained from SMHI (Swedish Meteorological Hydrological Institute) via SSPA (Swedish Maritime Research Centre). These data had some missing values. Therefore two continuous years were created out of the measured 25 months, replacing missing values with values from periods with equivalent weather conditions. The created years are shown in Figure 3.1 and Table 3.1a and b, where the mean energy fluxes are averaged over the actually measured values.

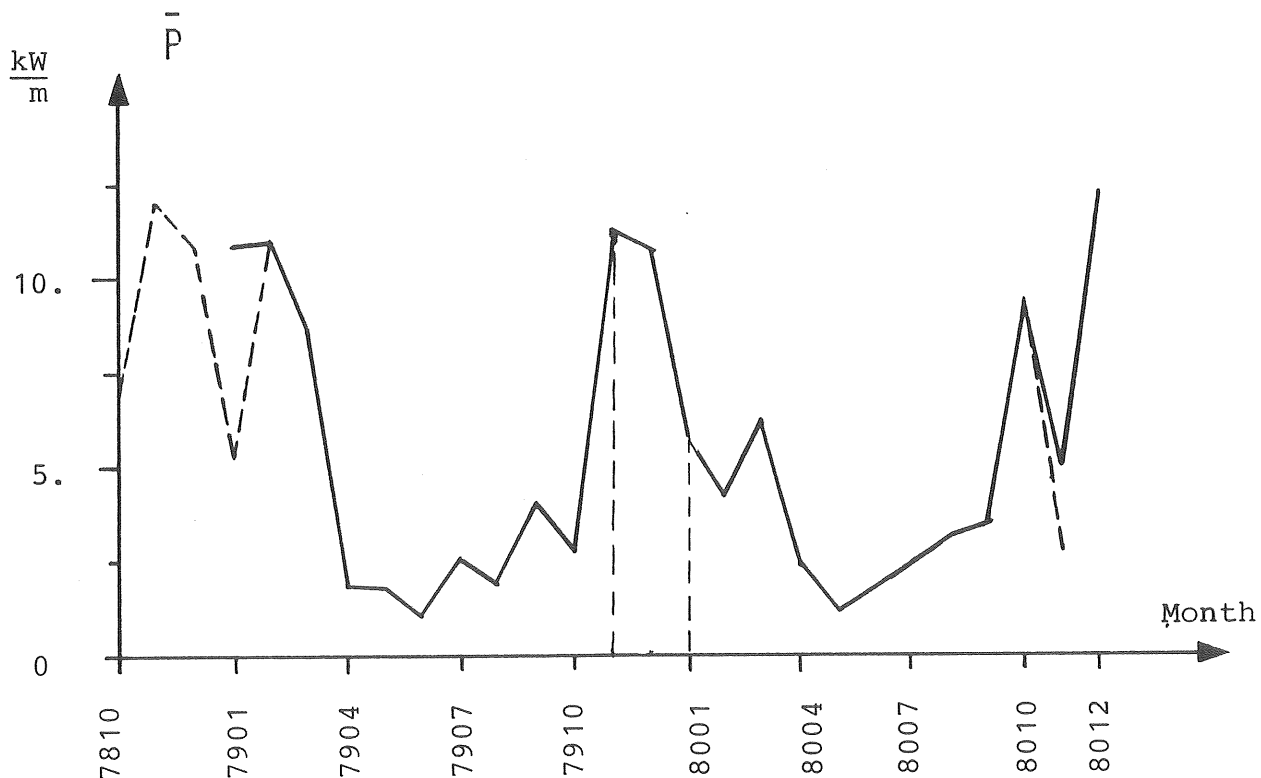


Figure 3.1 Mean energy flux. The dashed line is from the obtained (measured) series, and the solid line from the created series.

Table 3.1a Power means and number of hours each month.

Year	Month	\bar{P} (kW/m)	Number
1979	01	10.81	655
	02	11.00	593
	03	8.63	642
	04	1.82	636
	05	1.79	516
	06	1.00	661
	07	2.45	701
	08	1.93	718
	09	3.98	677
	10	2.84	711
	11	11.34	702
	12	10.79	656
1980	01	5.75	733
	02	4.05	635
	03	6.20	710
	04	2.21	682
	05	1.12	695
	06	1.46	665
	07	2.27	691
	08	3.00	604
	09	3.44	670
	10	9.25	484
	11	4.99	511
	12	12.15	668

The mean energy flux over the two years is

$$P = \frac{\sum \bar{P} \cdot N}{\sum N} = 5.1 \text{ kW/m}$$

where

\bar{P} is the power means from Table 3.1a and

N is their corresponding number of occurrences.

Table 3.1b

Means and standard deviations of the wave power (μ and σ), and the number of hours (N).
 Everything is for the created series and for the eight cardinal directions.

Year	Month	N			NE			E			SE			S			SW			W			NW		
		μ	σ	N	μ	σ	N																		
1979	01	2.4	1.3	39	5.1	10.7	148	19.8	29.1	250	6.0	4.8	115	5.4	4.6	67	1.4	0.0	1	7.0	2.9	28	3.0	1.6	7
	02	1.8	4.1	35	16.9	12.3	36	36.0	19.5	64	15.9	13.3	81	5.6	6.9	87	8.6	15.0	91	6.2	12.9	120	3.2	5.5	79
	03	2.6	1.6	42	24.5	35.6	117	5.7	6.2	50	1.7	1.0	21	5.6	6.5	125	6.4	6.3	200	3.3	3.9	76	1.2	0.8	11
	04	2.2	2.9	22	2.3	2.3	125	1.1	1.3	71	0.8	0.6	100	0.5	0.9	47	3.4	7.5	162	1.0	2.9	86	0.6	0.3	23
	05	0.8	0.9	8	0.3	0.5	10	0.6	0.9	20	1.4	2.8	79	0.8	1.4	99	3.1	6.3	197	0.9	0.9	86	1.0	1.0	17
	06	0.5	0.4	11	1.7	1.9	72	0.2	0.4	86	0.2	0.4	91	0.3	0.3	95	1.4	1.8	201	2.0	1.6	86	1.0	0.5	19
	07	0.7	0.5	32	0.6	0.1	9	0.3	0.1	4	0.3	0.2	9	0.2	0.3	16	2.7	3.6	176	3.1	3.3	363	0.8	0.7	92
	08	4.7	7.9	27	2.3	4.3	47	0.6	0.5	55	0.8	0.8	94	0.7	0.6	66	2.1	2.6	186	2.2	2.9	193	3.5	4.3	50
	09	1.2	1.0	35	0.1	0.1	11	0.1	0.0	7	0.1	0.1	30	0.2	0.2	42	6.8	7.2	205	4.3	5.3	267	1.1	1.3	80
	10	2.2	1.5	60	2.6	2.8	88	3.7	4.5	93	4.6	4.3	115	1.5	1.9	164	2.2	2.8	120	4.3	3.2	61	1.5	1.4	10
	11	4.2	2.8	50	4.0	1.6	4	3.4	2.5	42	6.4	5.3	71	11.1	9.9	117	18.0	25.3	246	8.5	17.1	133	7.4	6.8	39
	12	2.4	1.3	39	5.1	10.7	148	19.8	29.1	250	6.0	4.8	115	5.4	4.6	67	0.9	0.7	2	7.0	2.9	28	3.0	1.6	7
1980	01	7.9	7.7	145	3.3	4.3	65	2.4	2.7	82	5.4	5.1	98	7.1	7.9	103	6.4	5.5	69	4.5	3.8	89	6.8	7.4	82
	02	3.1	4.6	59	6.9	6.0	142	4.5	6.4	99	2.2	3.9	116	1.7	2.3	53	2.5	2.6	98	5.0	5.3	38	6.0	6.8	30
	03	9.3	4.3	36	5.9	6.1	122	5.3	4.8	179	8.7	8.3	206	1.8	1.0	46	2.4	1.3	50	4.0	1.9	47	9.5	5.0	24
	04	3.5	4.5	101	2.5	3.5	161	1.6	2.0	35	0.7	2.6	23	0.4	1.4	49	0.5	1.2	137	2.1	5.6	128	6.3	8.5	48
	05	1.2	1.4	78	2.1	2.1	206	0.6	0.7	84	0.5	0.3	49	0.3	0.3	49	0.8	1.3	138	0.4	0.4	53	0.6	0.7	38
	06	1.2	1.6	74	1.4	2.4	159	0.5	1.7	92	0.2	0.2	94	0.8	0.8	90	3.9	4.2	124	1.2	1.0	24	0.8	1.4	8
	07	2.8	5.3	66	0.7	0.6	187	0.5	0.4	91	0.5	0.4	42	0.6	1.0	58	2.9	4.6	124	6.3	8.1	95	6.6	8.2	28
	08	1.0	1.1	36	0.8	0.7	110	0.4	0.4	40	0.4	0.2	25	0.4	0.6	38	2.4	4.9	124	7.8	8.3	152	2.2	1.5	79
	09	3.8	6.4	33	5.2	9.1	73	0.6	0.4	12	0.5	0.5	32	2.1	4.4	136	4.5	6.8	179	4.5	7.1	130	1.6	2.0	75
	10	8.6	8.9	31	12.8	14.5	34	3.1	1.8	17	6.6	8.6	47	7.9	9.2	86	12.2	12.2	125	8.4	5.1	94	8.3	3.9	50
	11	5.0	2.8	60	1.9	1.2	75	2.0	0.8	82	1.8	1.0	9	3.1	1.7	8	8.4	12.1	59	6.5	9.7	136	6.3	4.2	82
	12	1.9	3.2	3	38.8	22.1	61	0.0	0.0	0	1.6	2.1	4	1.9	3.4	16	11.6	12.5	303	8.2	10.6	241	5.4	8.6	40

The year of 1979 has a greater energy flux than 1980;

$$\bar{P}_{79} = 5.7 \text{ kW/m}$$

$$\bar{P}_{80} = 4.6 \text{ kW/m}$$

Here the energy flux is defined as the flux into a circular cylinder of unit width and infinite in the vertical direction.

3.1.2 $H_s - T_z$ scatter diagrams

In the following scatter diagrams the number of hours for different seastates are presented as functions of H_s and T_z .

Here H_s and T_z are defined as, assuming a Rayleigh distribution

$$H_s = 4 m_0^{\frac{1}{2}} = 4 \left(\sum_{i=5}^{42} S_i \Delta\omega \right)^{\frac{1}{2}} \quad (3.1)$$

and

$$T_z = T_2 = 2\pi \left(\frac{m_0}{m_2} \right)^{\frac{1}{2}} = 2\pi \left(\frac{\sum_{i=5}^{42} S_i \Delta\omega}{\sum_{i=5}^{42} \omega_i^2 S_i \Delta\omega} \right)^{\frac{1}{2}}$$

where

S_i is the spectral density

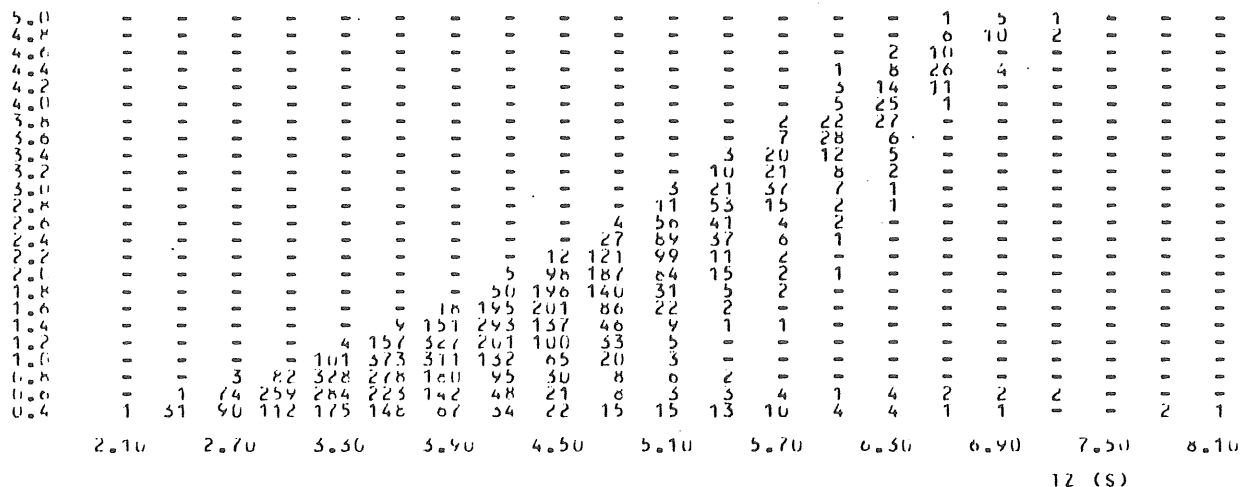
ω_i is the angular frequencies (Chapter 2)

$\Delta\omega = 2\pi/64$ rad/s.

Figure 3.2 contains scatterdiagrams for all data 1979-1980. In Figures 3.3-3.5 the scatterdiagrams for each month are splitted on the eight cardinal wind directions. The direction of propagation of waves is considered to be the same as the wind direction.

Fig. 3 .2 Scatterdiagrams for all wind directions.

HS (m)

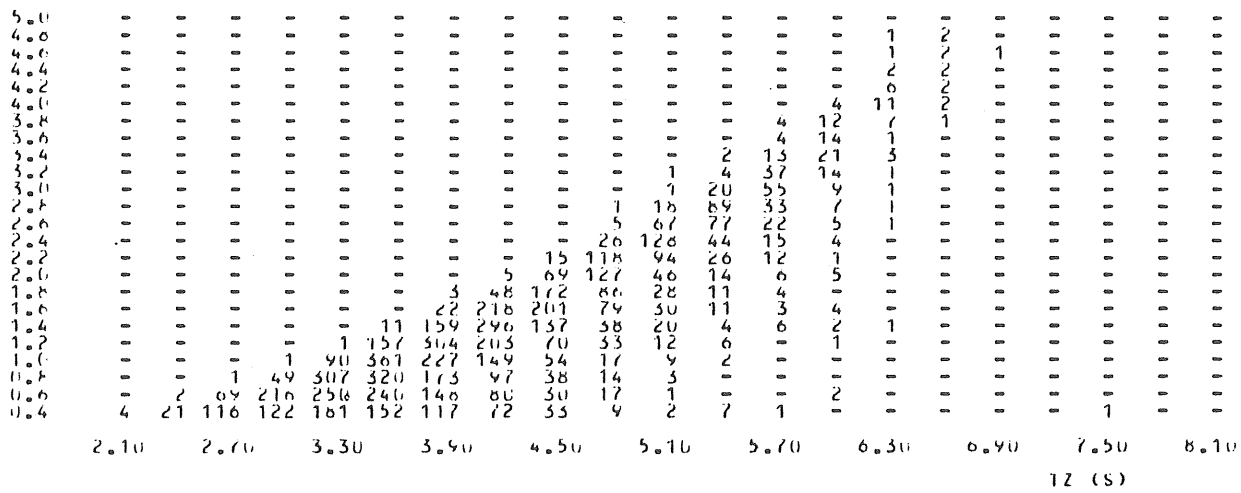


HS=12=0.0

200 HOURS

1979

HS (m)

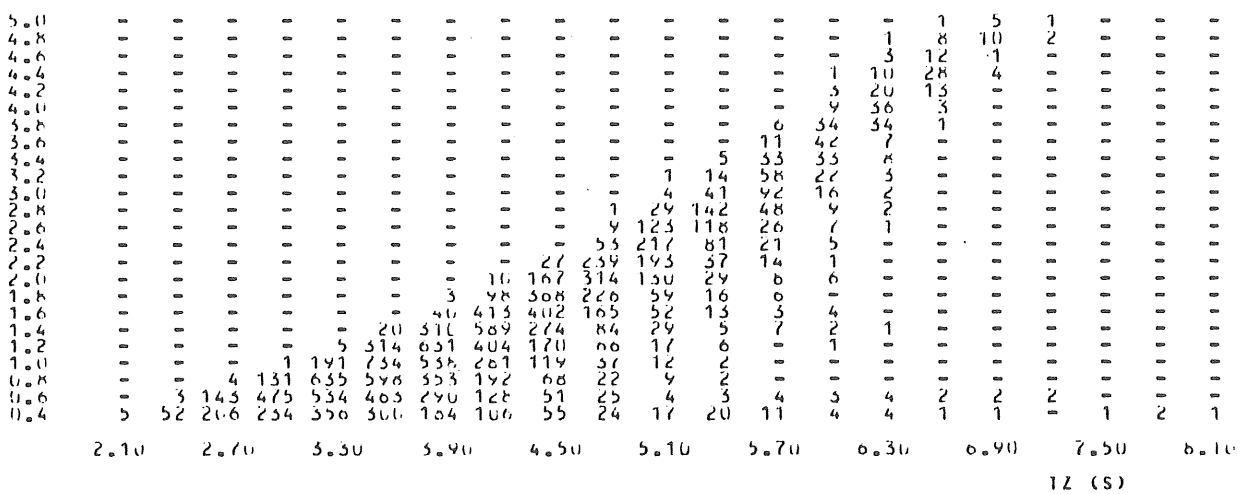


HS=12=0.0

218 HOURS

1980

HS (m)



TOTAL

HS=12=0.0

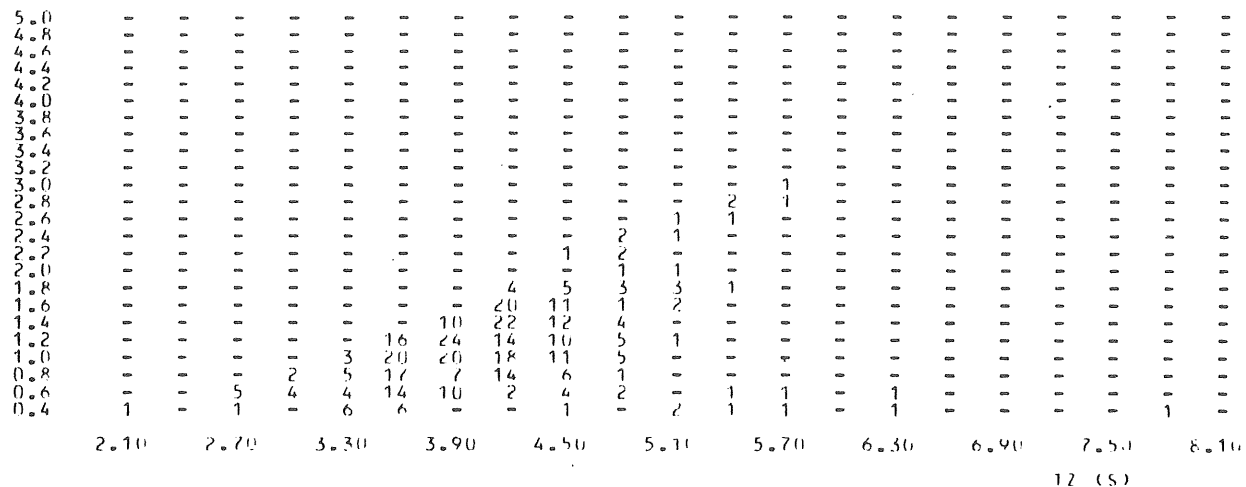
418 HOURS

SCATTERDIAGRAM FOR WINDDIRECTION: N

Fig. 3.3 a

YEAR: 1979

HS (M)



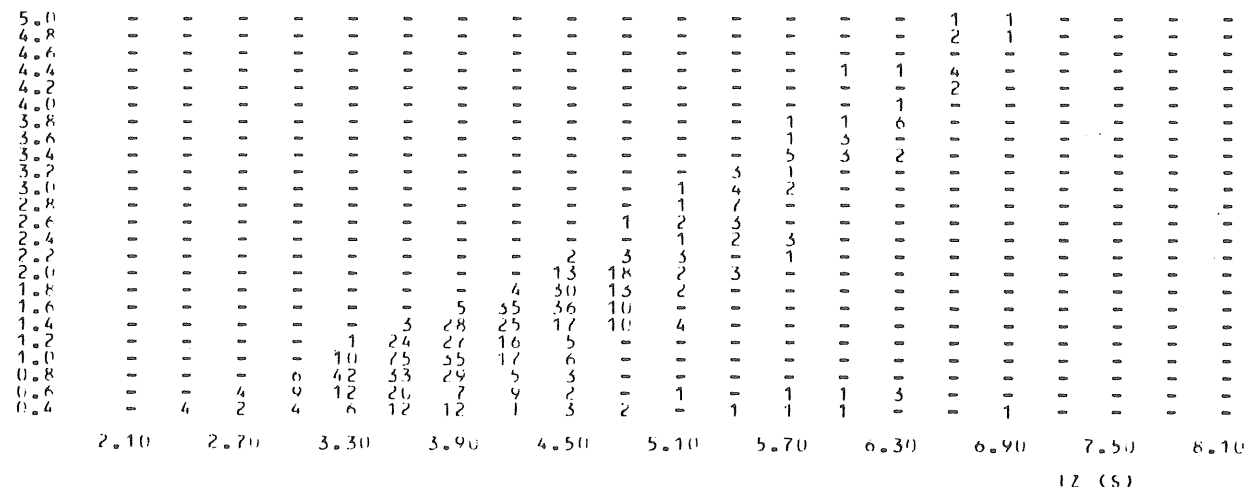
HS=TZ=0.0

20 HOURS

SCATTERDIAGRAM FOR WINDDIRECTION: NE

YEAR: 1979

HS (M)



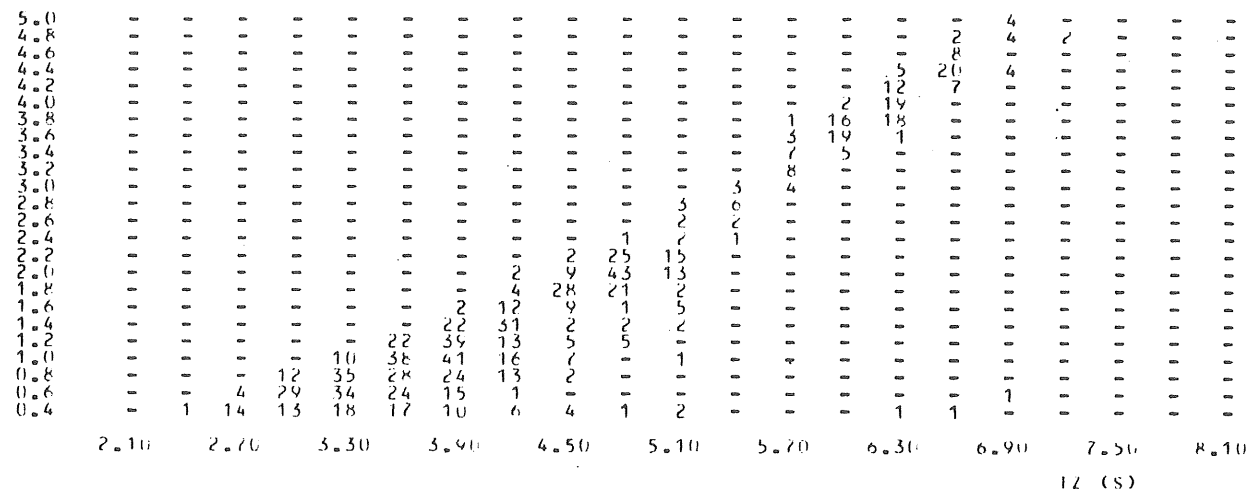
HS=TZ=0.0

15 HOURS

SCATTERDIAGRAM FOR WIND DIRECTION: E

YEAR: 1979

HS (m)



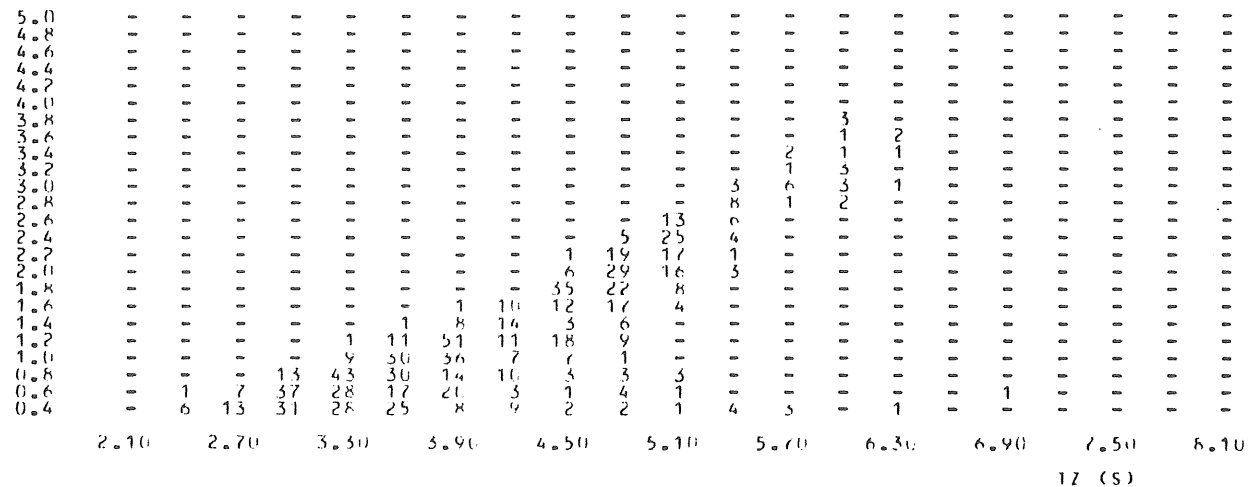
HS=TZ=0.0

30 HOURS

SCATTERDIAGRAM FOR WIND DIRECTION: SE

YEAR: 1979

HS (m)



HS=TZ=0.0

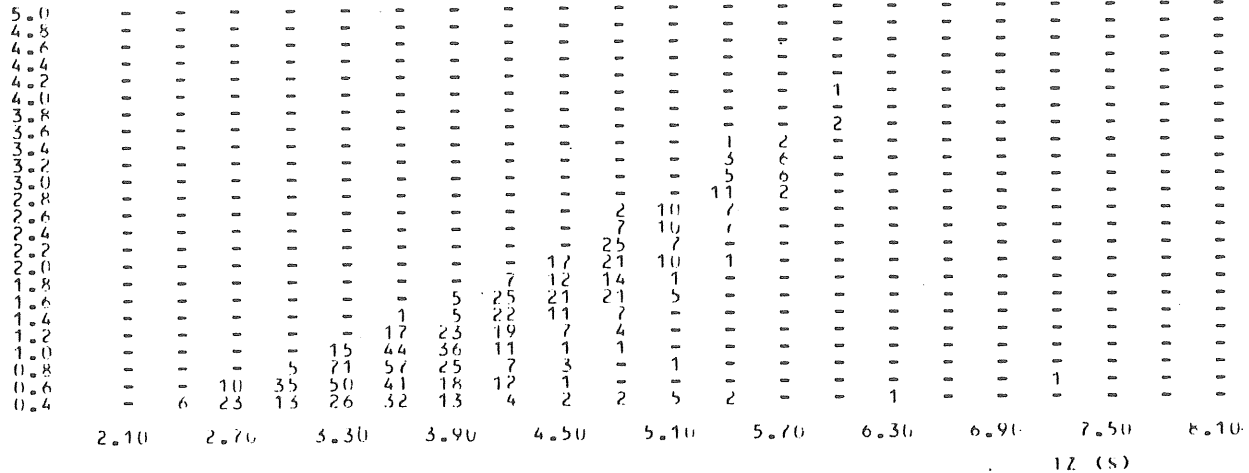
34 HOURS

Fig. 3.3 b

SCATTERDIAGRAM FOR WINDDIRECTION: S

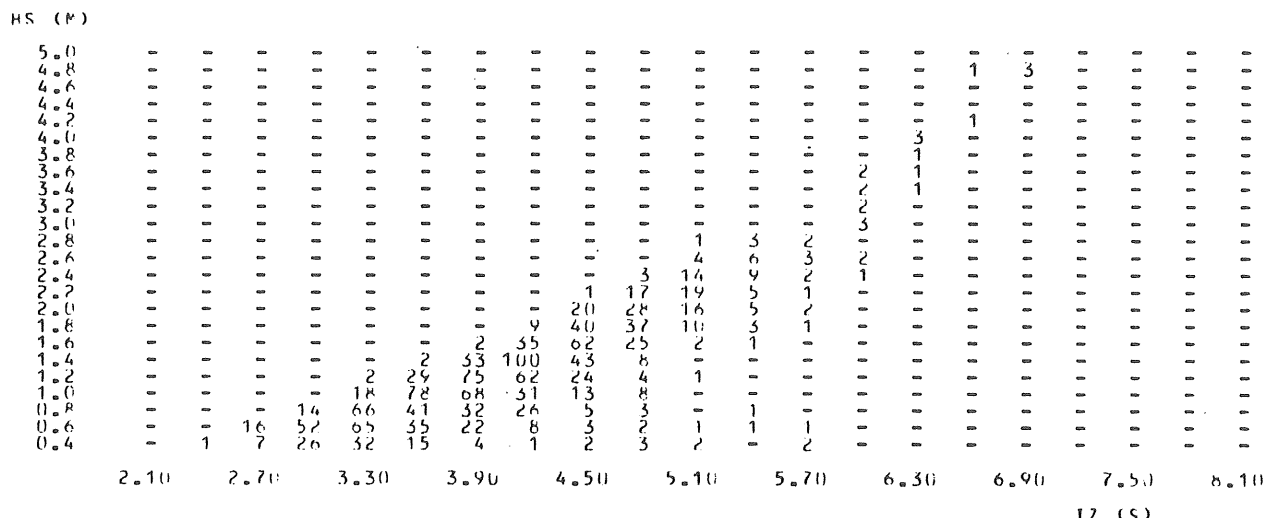
YEAR: 1979

HS (m)



SCATTERDIAGRAM FOR WIND DIRECTION: W

YEAR: 1979

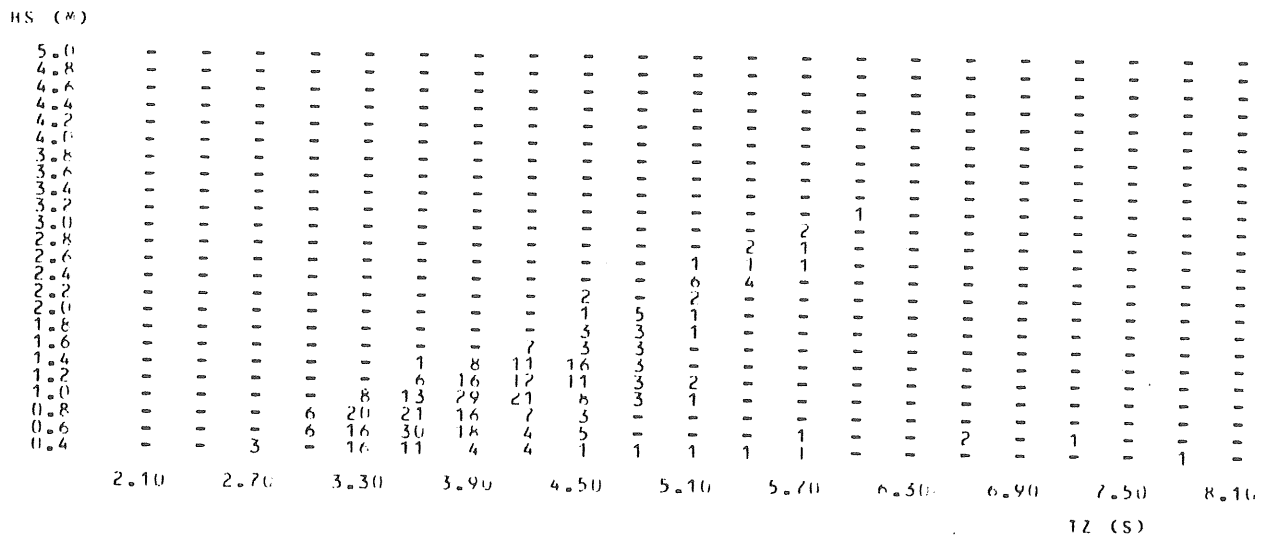


HS=TZ=0.0 27 HOURS

Fig. 3.3 d

SCATTERDIAGRAM FOR WIND DIRECTION: NW

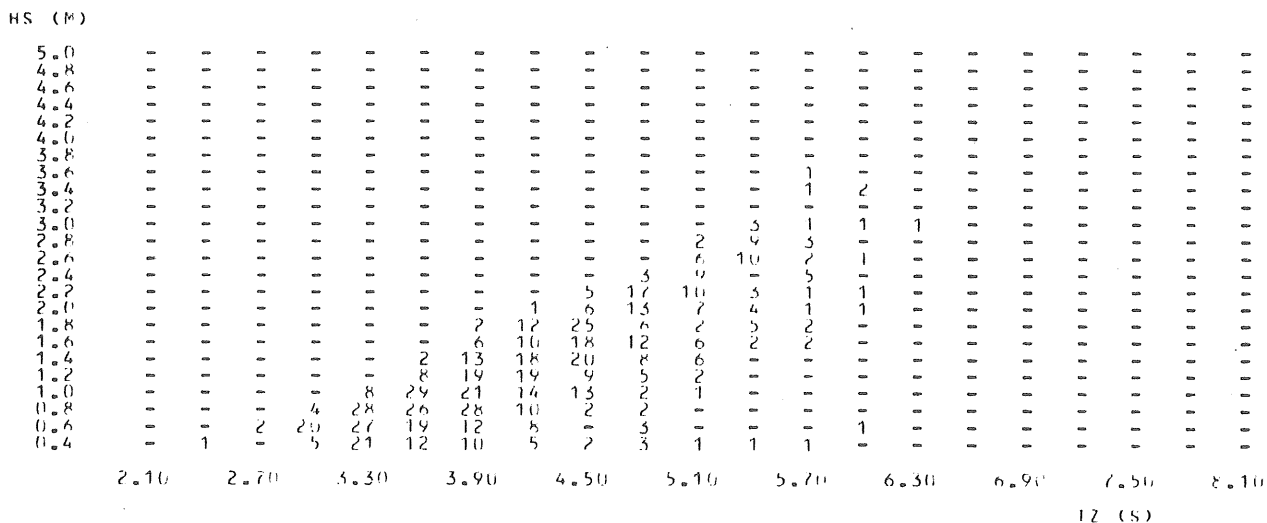
YEAR: 1979



HS=TZ=0.0 12 HOURS

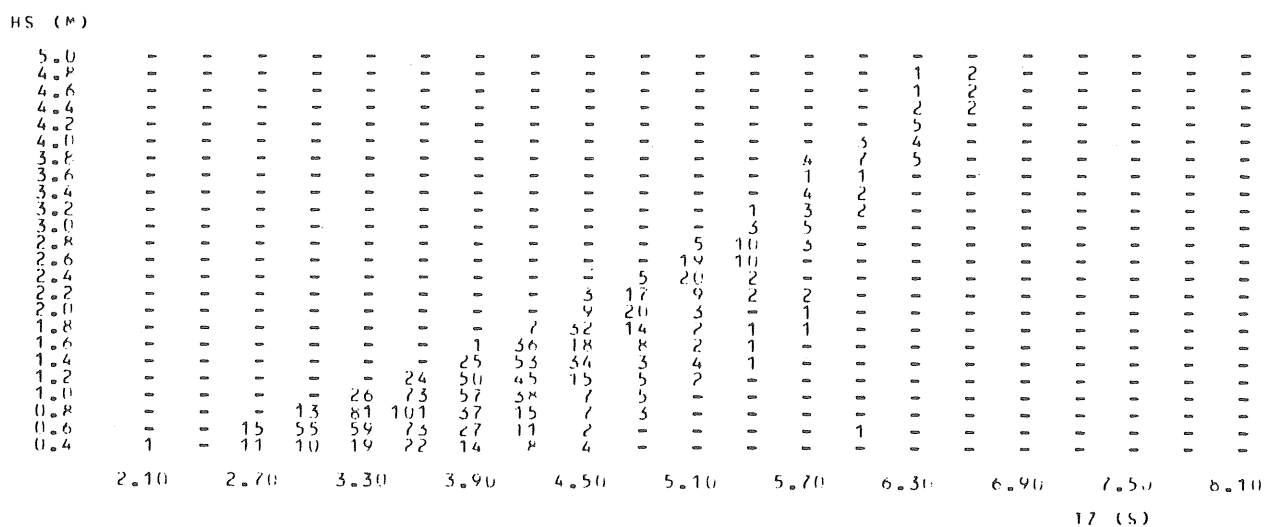
SCATTERDIAGRAM FOR WIND DIRECTION: N

YEAR: 1980

Fig. 3.4 a

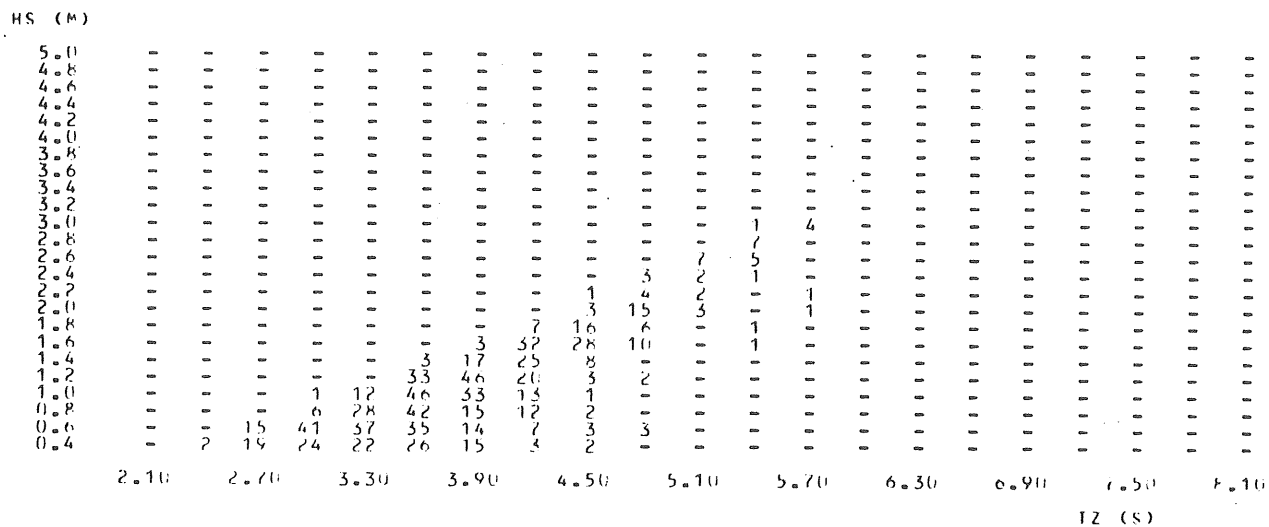
SCATTERDIAGRAM FOR WIND DIRECTION: NE

YEAR: 1980



SCATTERDIAGRAM FOR WIND DIRECTION: E

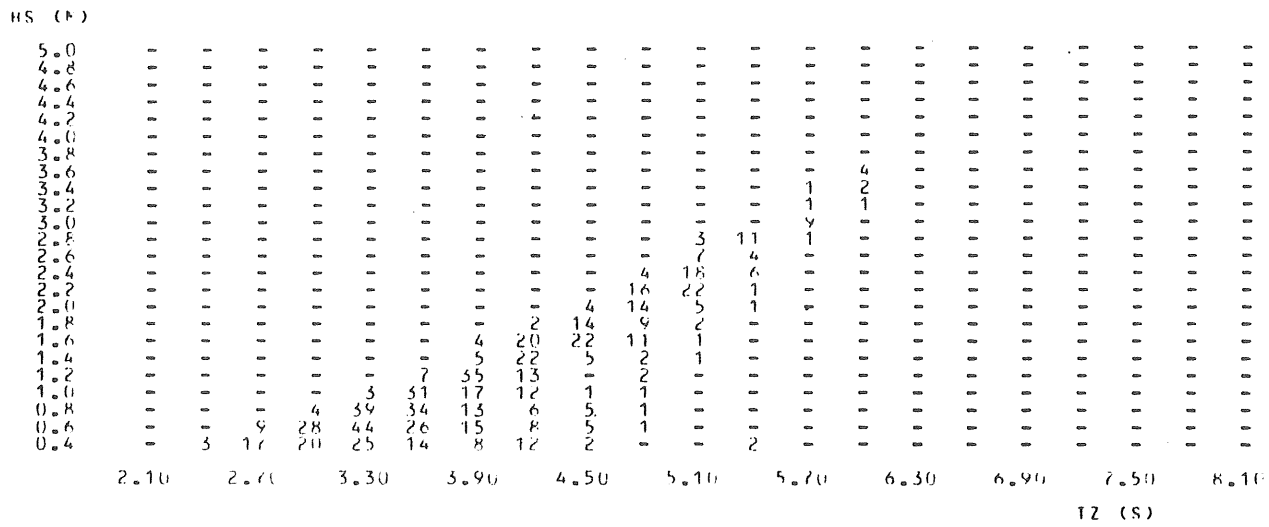
YEAR: 1980

Fig. 3.4 b

HS=TZ=0.0 11 HOURS

SCATTERDIAGRAM FOR WIND DIRECTION: SE

YEAR: 1980



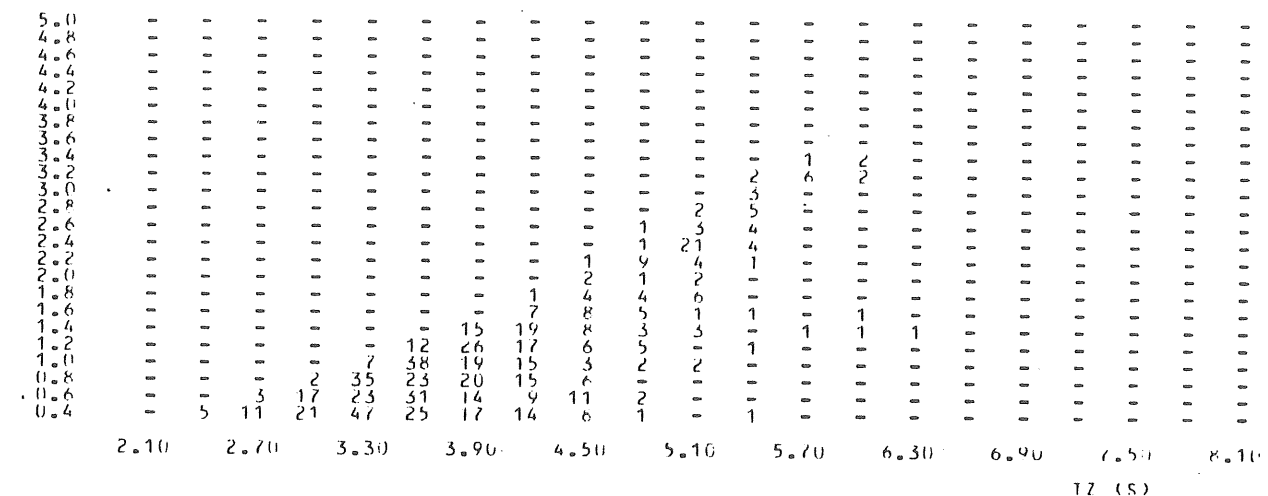
HS=TZ=0.0 27 HOURS

SCATTERDIAGRAM FOR WIND DIRECTION: S

YEAR: 1980

Fig. 3.4 c

HS (m)



HS=TZ=0.0

77 HOURS

SCATTERDIAGRAM FOR WIND DIRECTION: SW

YEAR: 1980

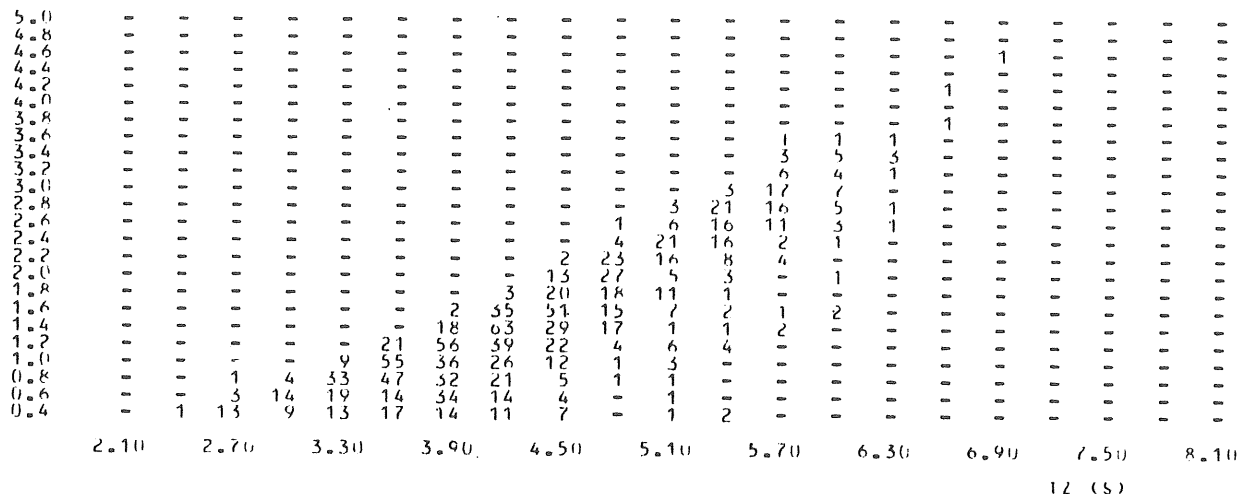
Fig. 3.4 c

SCATTERDIAGRAM FOR WINDDIRECTION: W

YEAR: 1980

Fig. 3 . 4 d

HS (m)



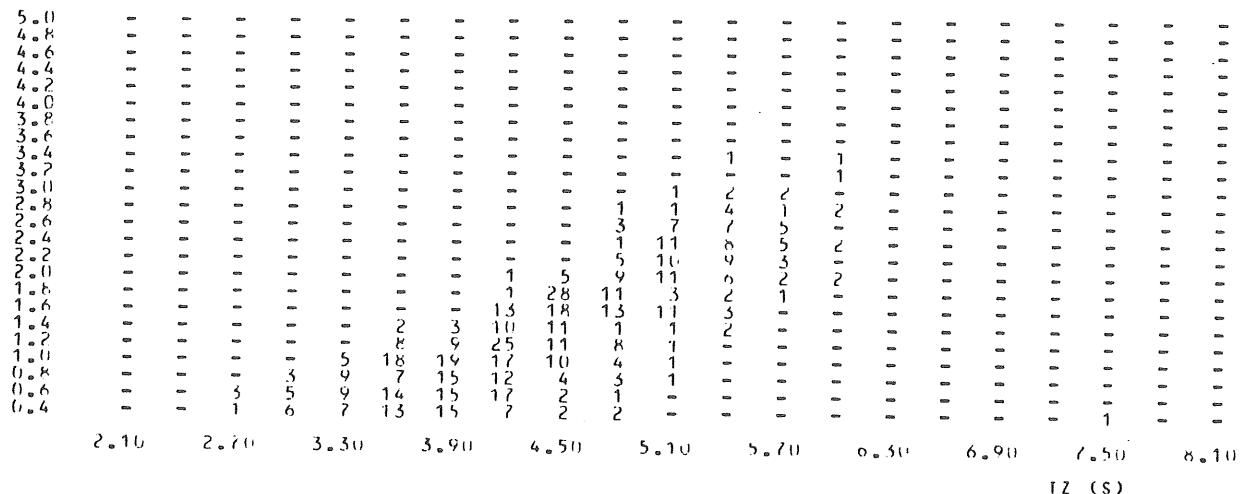
HS=1Z=0.0

13 HOURS

SCATTERDIAGRAM FOR WINDDIRECTION: NW

YEAR: 1980

HS (m)



HS=1Z=0.0

13 HOURS

SCATTERDIAGRAM FÜR WINDDIRECTION: N

TOTAL

HS (M)

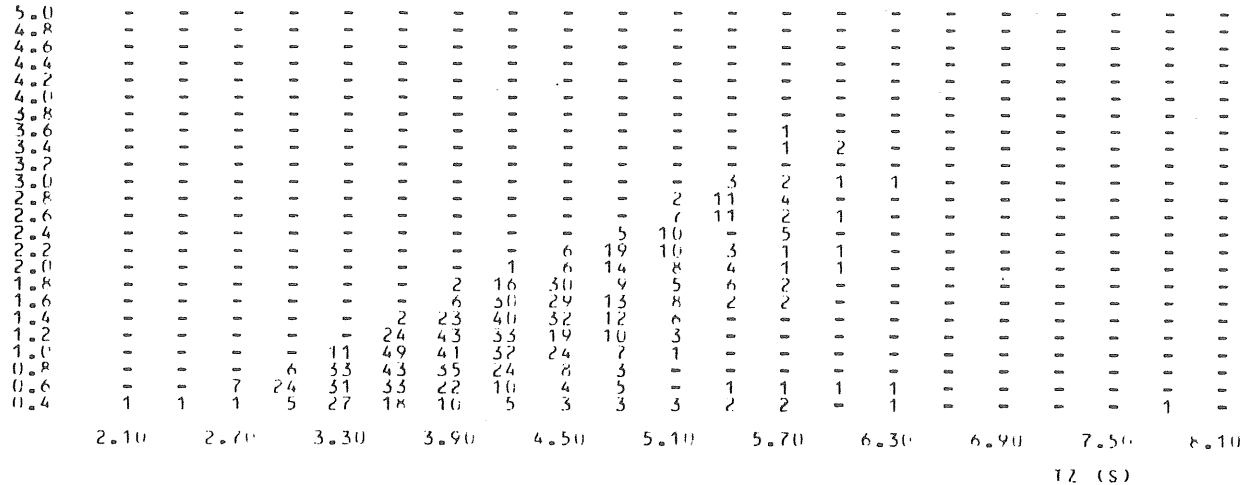


Fig. 3.5 a

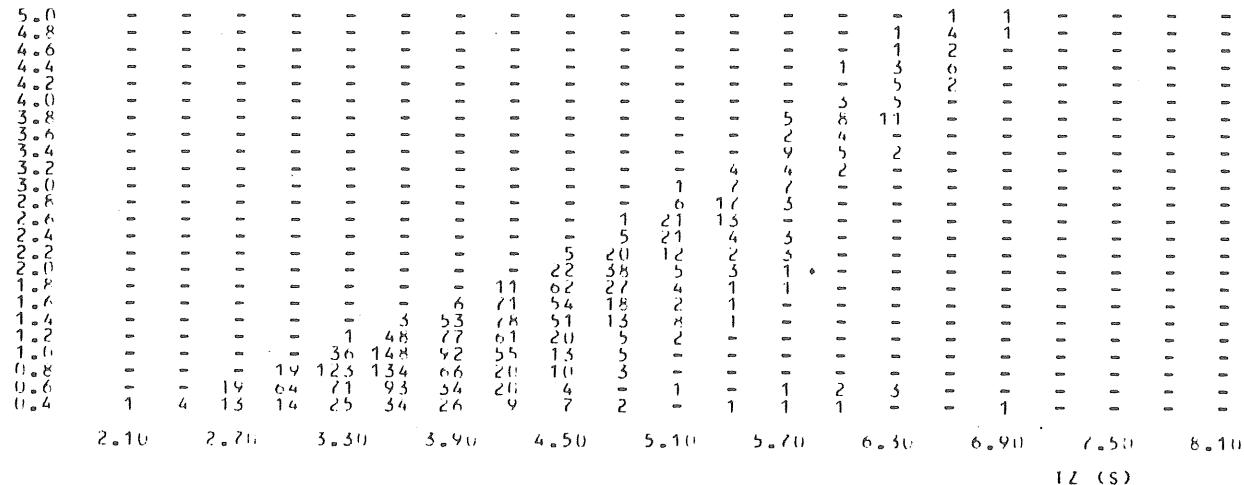
HS=TZ=0.0

31 HOURS

SCATTERDIAGRAM FÜR WINDDIRECTION: NE

TOTAL

HS (M)



HS=TZ=0.0

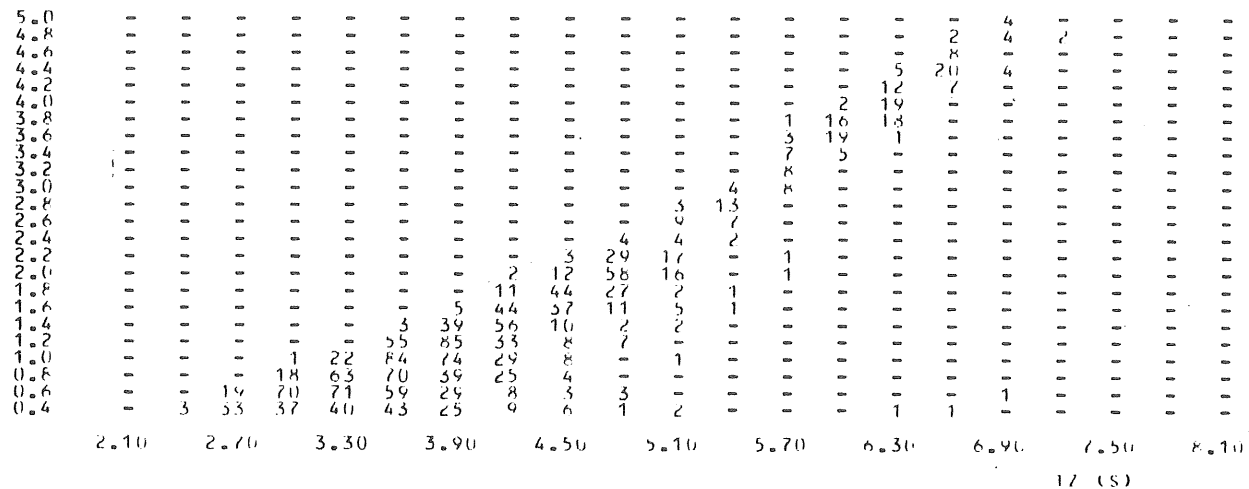
31 HOURS

SCATTERDIAGRAM FOR WINDDIRECTION: E

TOTAL

Fig. 3.5 b

HS (M)



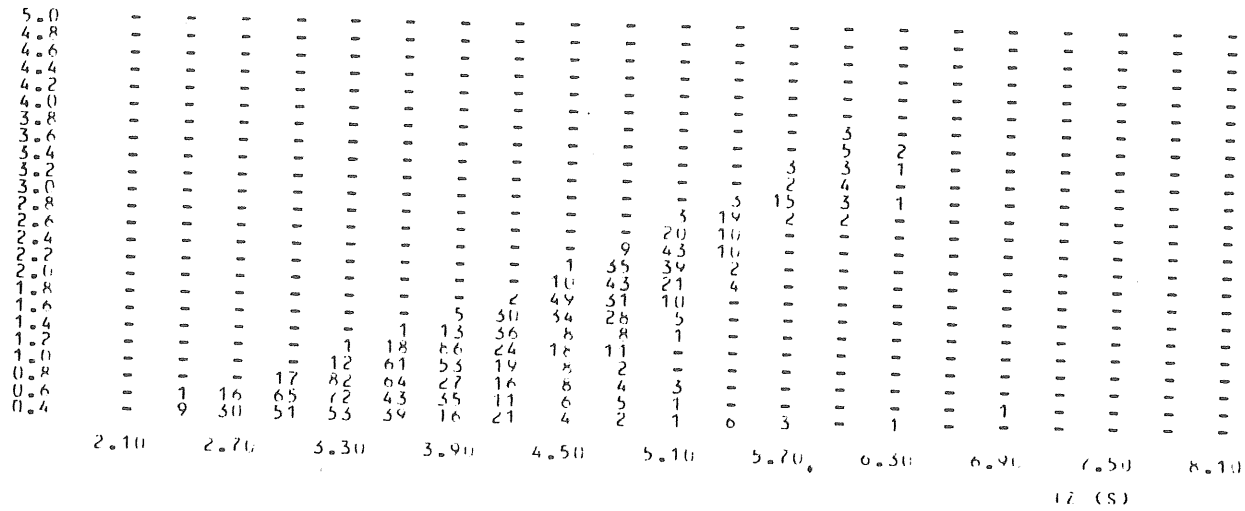
HS=TZ=0.0

41 HOURS

SCATTERDIAGRAM FOR WINDDIRECTIONS: SE

TOTAL

HS (M)



HS=TZ=0.0

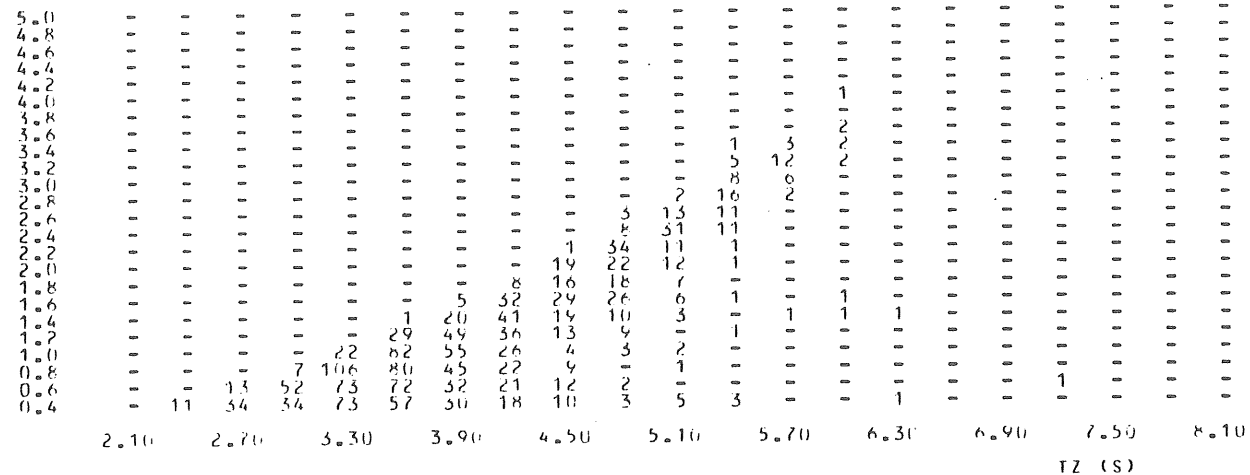
61 HOURS

SCATTERDIAGRAM FOR WIND DIRECTION: S

TOTAL

Fig. 3.5 C

HS (m)



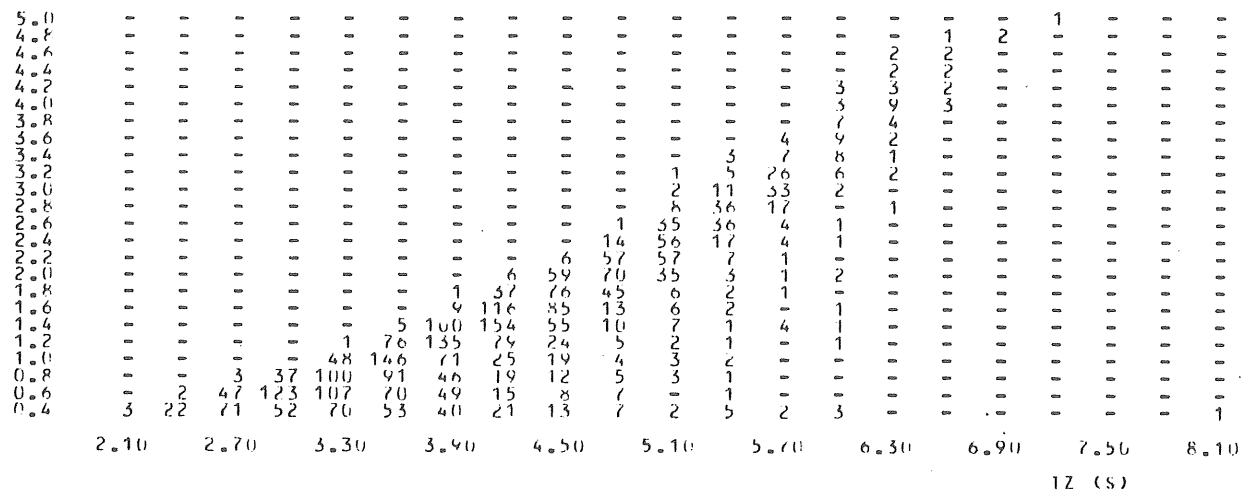
HS=TZ=0.0

74 HOURS

SCATTERDIAGRAM FOR WIND DIRECTION: SW

TOTAL

HS (m)



HS=TZ=0.0

112 HOURS

SCATTERDIAGRAM FOR WIND DIRECTION: W

TOTAL

HS (M)

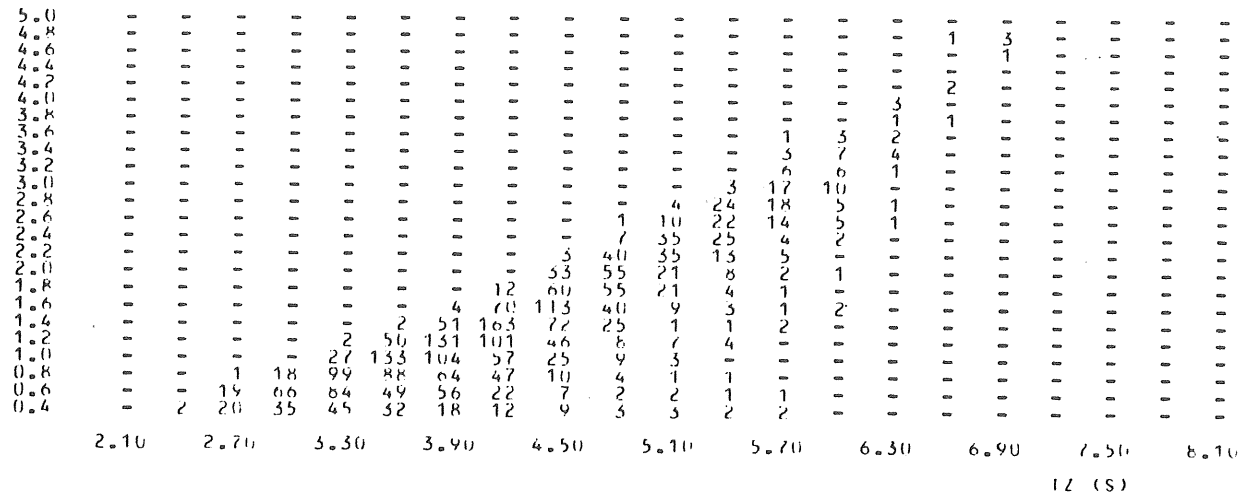


Fig. 3.5 d

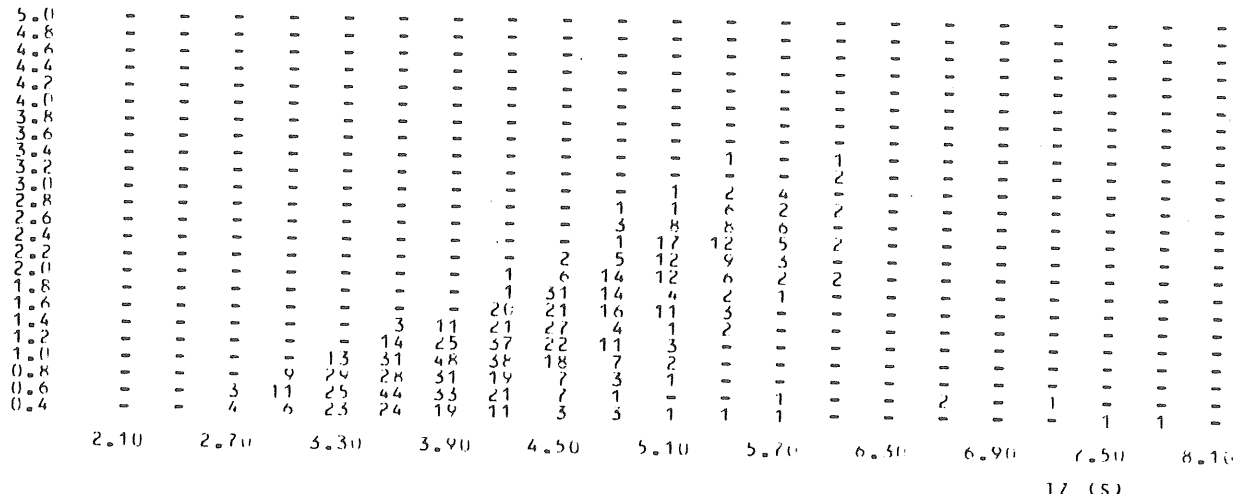
HS=1Z=0.0

40 HOURS

SCATTERDIAGRAM FOR WIND DIRECTION: NW

TOTAL

HS (M)



1Z (S)

HS=1Z=0.0

23 HOURS

3.1.3 H_s - T_z relation

Performing a regression analysis (equivalent to that in Chapter 4.3) and assuming the following relation

$$H_s = C T_z^2 \quad (3.3)$$

The best fit is when

$$C = \frac{\sum H_{si}}{\sum T_{zi}^2} \quad (3.4)$$

The correlation coefficient from Eq. (4.11) is

$$R = \frac{\sum H_{si}}{\sum T_{zi}^2} \left(\frac{\sum T_{zi}^4}{\sum H_{si}^2} \right)^{\frac{1}{2}} \quad (3.5)$$

An analysis of the wave data gives the results shown in Table 3.2. The results indicate quite a good correlation between H_s and T_z^2 .

Comparing C with the value for a FAS stated by the PM-spectrum for which $C_{PM}=0.103$, indicates that the sea state is very seldom near fully arisen. (Compare Figure 4.13.)

Table 3.2 does not imply any major correlation between C and the geographical fetch. There is a tendency, though, that C is somewhat smaller in the northwestern direction.

As an average relation between H_s and T_z the following expression can be used.

$$\overline{H_s} = 0.06 \overline{T_z^2} \quad (3.6)$$

This equation can be used in comparing it with equivalent expressions for other ocean areas. Then it can give an indication of the probability of a FAS condition to occur.

Table 3.2 Regression analysis results (Eqs. 3.3-3.5).

Year	Dir.	C	R	Hours
1979	N	0.052	0.87	400
	NE	0.064	0.76	806
	E	0.071	0.86	982
	SE	0.058	0.87	921
	S	0.058	0.85	991
	SW	0.064	0.87	1782
	W	0.060	0.91	1526
	NW	0.048	0.89	434
	A11	0.062	0.86	7842
1980	N	0.059	0.90	722
	NE	0.061	0.85	1395
	E	0.057	0.88	811
	SE	0.059	0.86	745
	S	0.050	0.82	732
	SW	0.066	0.88	1530
	W	0.063	0.90	1227
	NW	0.058	0.90	584
	A11	0.060	0.87	7746
Both	N	0.057	0.90	1122
	NE	0.062	0.86	2201
	E	0.066	0.84	1793
	SE	0.059	0.87	1666
	S	0.055	0.84	1723
	SW	0.065	0.88	3312
	W	0.062	0.91	2753
	NW	0.054	0.89	1018
	A11	0.061	0.87	15588

3.2 Energy flux

3.2.1 Energy flux probability

The mean energy flux for the two years is 5.1 kW/m. This value is exceeded with a probability of 25%. Other fractiles of interest are

$$50\%: P = 1.5 \text{ kW/m}$$

$$10\%: P = 14.0 \text{ kW/m}$$

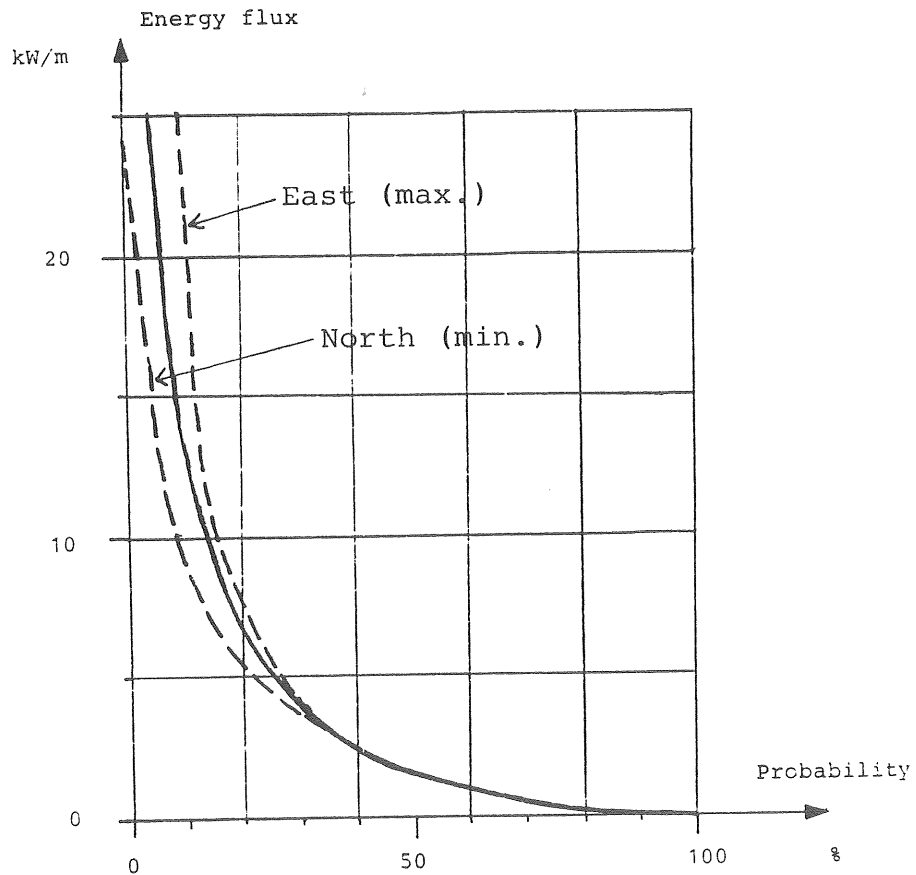


Figure 3.6 Wave energy flux versus probability of occurrence. The solid line is the average and the dashed lines are minimum and maximum. (Wave data from O.S.G.)

The maximum and minimum lines in Figure 3.6 are for easterly and northerly directions, respectively. As the power exceeds 3.4 kW/m, these start to differ from the average. Below this limit there are very small differences.

3.2.2 $P - H_s^2 T_z$ relation

Two methods can be used when calculating the wave power; the spectrum method and the wave parameter method, which both are presented below.

Spectrum method:

$$P = \frac{\rho g}{2\pi} \sum_i \frac{S(f_i)}{f_i} \Delta f \quad (3.7)$$

Here $S(f_i)$ is the spectral density as a discrete function of the frequency, f

$$\rho = 1005 \text{ kg/m}^3; \text{ water density}$$

$$g = 9.81 \text{ m/s}^2$$

The used spectral density and frequency discretization are accounted for in Chapter 2.

If only H_s and T_z are available (the most common case) then the wave parameter method should be used.

$$P = A H_s^2 T_z \quad (3.8)$$

Inserting Eq. (3.7) into Eq. (3.8) and using values for ØSG, gives

$$A = 520 \pm 20 \text{ W/m}^3\text{s}$$

which gives the equation to be used

$$P = 0.52 H_s^2 T_z \text{ (kW/m)} \quad (3.9)$$

A performed sensitivity analysis indicated that A was uncorrelated to both the mean wind speed and the wind direction.

The values of A has been investigated for the Norwegian North Sea coast by Gran (1977). The North Sea waves gave

$$A_{NS} = 550 \pm 40 \text{ W/m}^3\text{s}$$

which is slightly higher than for ØSG. This indicates a higher amount of lower frequency waves in the North Sea.

For theoretical standard spectra A ranges between 500-590 $\text{W/m}^3\text{s}$. For a PM spectrum the value of A is

$$A_{PM} = 580 \text{ W/m}^3\text{s}$$

3.2.3 Accumulated wave energy distributions

Although the wave parameter method appears to be a good approximation the spectral method should be used if there are some spectral data available. As far as this, the discussions have only included power averages and variances. If it shall be possible to estimate the distribution in the frequency domain, power spectra must be used.

One way to describe the longterm distribution of the energy in the frequency domain, is presented in Figure 3.7. These are the distribution of the accumulated energy distributions as functions of direction and frequency.

The mean wave period over a year is 7.7 s and the tendency is that with increasing spectrum peak values the peak frequency decreases.

Major energy contents are in the easterly and southwesterly directions. Here the easterly spectra contain more energy in the low frequency.

If the accumulated wave spectra are to be used when comparing different wave energy devices, it shall be noticed that some kind of accumulated energy transfer function has to be used. Or assuming the device to be linear in its energy conversion.

When using the cardinal directions, it shall be noticed, that the dispersive directionality of the sea must be considered, this can decrease the efficiency of unidirectional wave energy absorbers.

4 GEOGRAPHICAL DISTRIBUTION OF WAVE ENERGY

4.1 Introduction

Sweden has no ocean coast and therefore the heights and periods of the waves are rather limited. Maximum zero upcrossing periods are about $T_z = 10$ s and maximum significant heights, $H_s = 5$ m. The mean wave energy flux in Swedish water are less than 6 kW/m, to be compared with the Scottish Atlantic coast, where the mean is 50 kW/m.

Swedish waters with the most wave energy are the Southern Baltic and the Skagerrak. In these waters the mean energy flux is about 6 kW/m.

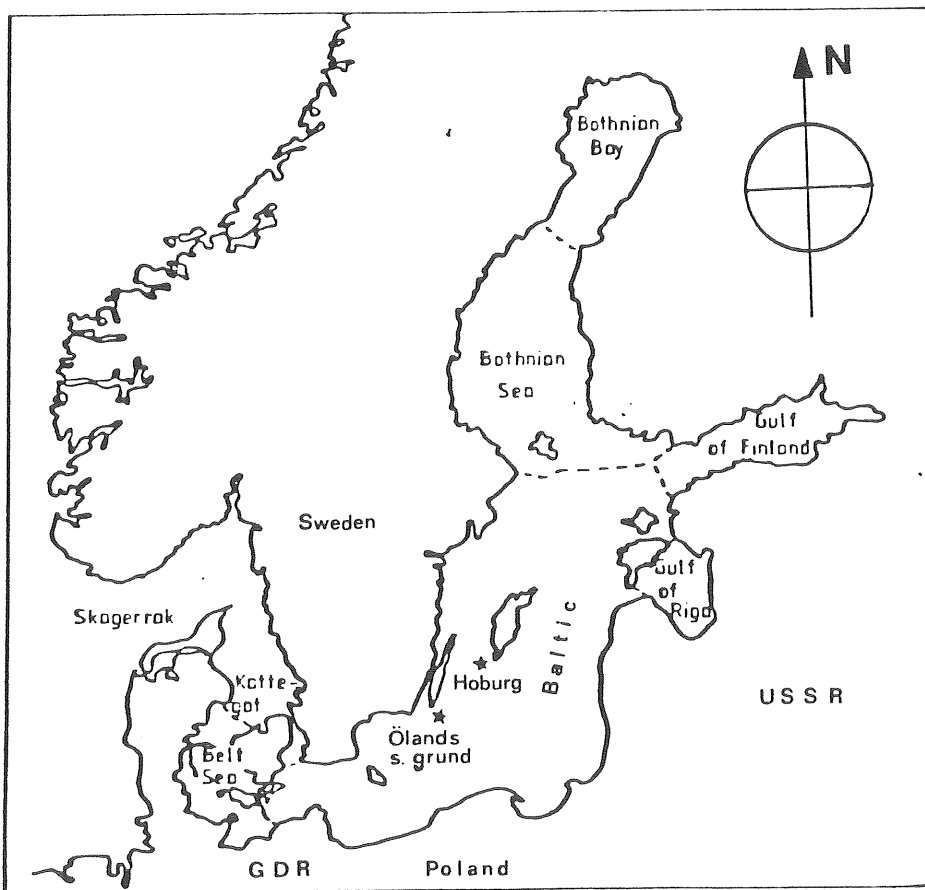


Figure 4.1 Measuring sites in the southern Baltic, at Ölands södra grund and Hoburg.

The measuring sites of interest when dealing with the Southern Baltic, are: Ölands södra grund (south of the island of Öland) and Hoburg (south of the island of Gotland), see Figure 4.1.

Looking at the map (Figure 4.1) one would expect that there should be more wave energy at Hoburg than at Ölands södra grund (ÖSG) and this was the belief when starting this investigation.

Hindcasts (calculations of waves out of winds) done for one year period (Rylander (1978)) show that there would be more energy at Hoburg.

SMHI's measurements indicated the opposite. According to these measurements, there is about 30% more energy at ÖSG than at Hoburg, for a period from June 1981 to February 1982. This fact arouses the question: Is there ordinarily more energy at ÖSG?

The following paragraphs 4.2-4.3 give possible explanations for the difference between the two measuring locations.

4.2 Wave generation aspects

4.2.1 Wind climate

One reason why there is less wave energy at Hoburg, is that the mean wind speed is lower, see Figure 4.2.

Average wind speeds are, at

$$\begin{aligned} \text{ÖSG: } \bar{U}_{10} &= 8.32 \text{ m/s} \\ \text{Hoburg: } \bar{U}_{10} &= 7.09 \text{ m/s} \end{aligned}$$

Another reason is that the average fetch available, due to the limiting coasts of the Baltic, is just about equal for both places, and not larger at Hoburg. The average fetches due to geographical limitations are, at

$$\begin{aligned} \text{ÖSG: } \bar{F}_A &= 160 \text{ km} \\ \text{Hoburg: } \bar{F}_A &= 145 \text{ km} \end{aligned}$$

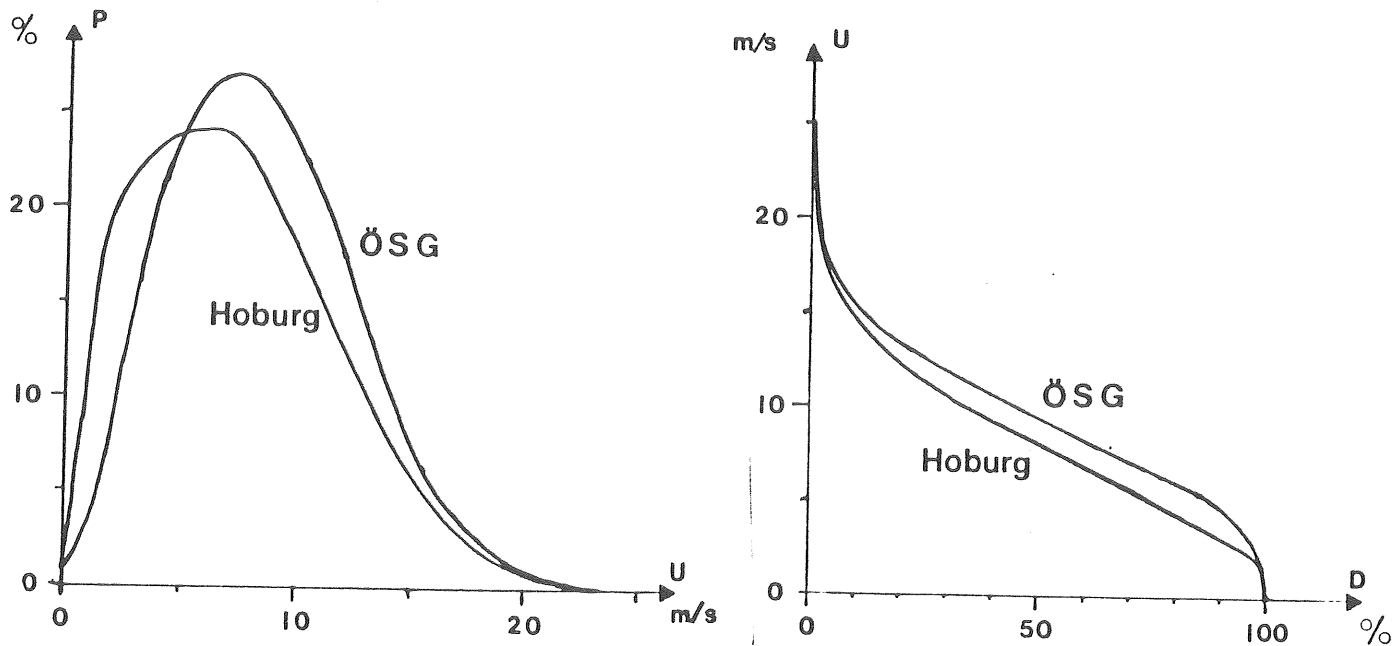


Figure 4.2a The probability, p , of the occurrence of wind speeds, U .

Figure 4.2b Cumulated probability versus wind speed.

(Source: Wind data from lighthouses at Ölands södra udde and Hoburg. Measured by SMHI 1961-1975.)

Directionality of the wind is an important parameter. The main wind direction in this area is south-west. It is possible to derive the directional distribution of the wind at the two lighthouses, Table 4.1, from the wind data for the years 1961-1975.

Table 4.1 Mean wind speeds, \bar{U} , for stations Ölands södra udde and Hoburg. (Years: 1961-1975)

ÖLANDS SÖDRA UDDE

	\bar{U}	$\bar{U^2}$	$\bar{U^3}$	$\bar{1/U}$	$\bar{1/U^2}$
Dir.	m/s	m^2/s^2	m^3/s^3	s/m	s^2/m^2
N	7.10	65.0	714.	0.204	0.066
NE	7.96	77.4	862.	0.174	0.049
E	7.74	74.1	828.	0.179	0.051
SE	7.52	72.8	826.	0.200	0.067
S	7.48	72.9	842.	0.206	0.072
SW	9.51	109.	1420.	0.145	0.036
W	9.38	106.	1380.	0.145	0.035
NW	7.33	69.1	782.	0.199	0.064

HOBURG

	\bar{U}	$\bar{U^2}$	$\bar{U^3}$	$\bar{1/U}$	$\bar{1/U^2}$
Dir.	m/s	m^2/s^2	m^3/s^3	s/m	s^2/m^2
N	7.02	70.9	886.	0.253	0.110
NE	6.17	54.5	587.	0.283	0.131
E	6.47	56.8	595.	0.254	0.108
SE	6.78	64.1	731.	0.255	0.111
S	6.78	65.2	762.	0.258	0.113
SW	7.97	83.3	1020.	0.205	0.076
W	7.68	78.7	960.	0.215	0.083
NW	6.62	63.5	766.	0.265	0.118

The energy flux in the wind fields is, as an approximation, proportional to the wind speed cubed.

$$P_w \sim U^3 \quad (4.1)$$

In Figure 4.3 the directional distribution of the mean wind speed and the mean wind power are graphed as wind roses. The southwesterly domination is clearly pronounced for the energy flux, especially for ØSG.

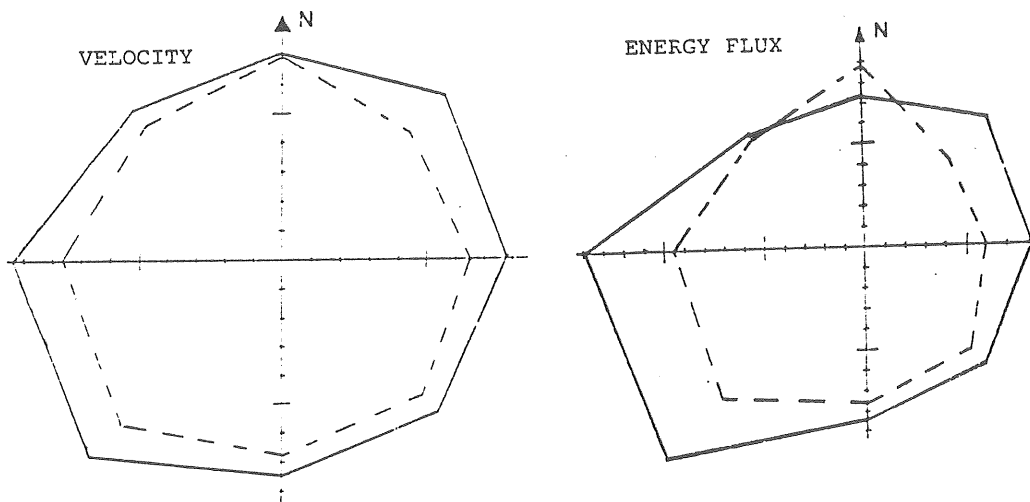


Figure 4.3 The directional distribution of the average wind velocity and the average wind energy flux, according to Table 4.1. (ØSG - solid line, Hoburg - dashed line)

Comparing ØSG and Hoburg gives that the mean wind power is about 30% greater at ØSG. The average of the cubed wind speed is, at;

$$\text{ØSG: } \overline{U_{10}^3} = 1050 \text{ m}^3/\text{s}^3$$

$$\text{Hoburg: } \overline{U_{10}^3} = 826 \text{ m}^3/\text{s}^3$$

4.2.2 Efficient fetches

This far, the only thing considered is the wind speed. It is also of interest if the sea can be regarded as fetch-limited or not. In Hasselmann et al (1973), where the JONSWAP spectrum is presented, Phillips constant α is expressed using only the fetch, F , and wind speed, U_{10} , at the 10 m level above sea surface.

$$\alpha = 0.076 F_0^{-0.22} \quad (4.2)$$

where

$$F_0 = gF/U_{10}^2 \quad (4.3)$$

If the sea is a FAS (fully arisen sea) Phillips constant is

$$\alpha_{FAS} = 8.1 \cdot 10^{-3} \quad (4.4)$$

or less.

With Eqs. (4.3) and (4.4) substituted into Eq. (4.2) it is possible to calculate the fetch required for a FAS, F_{FAS} , with the wind speed as the only parameter.

$$F_{FAS} = \left(\frac{\alpha_{fas}}{0.076} \right)^{-4.55} \frac{U_{10}^2}{g} \quad (4.5)$$

or

$$F_{FAS} = 2680 U_{10}^2 \quad (4.6)$$

As the available fetches for the two wave measuring sites are known, it is possible to calculate whether the average wind creates a fetch limited sea or not, see Table 4.2.

Table 4.2 Directional distribution of the average efficient fetch, for wind data from Table 4.1.

In the table \bar{F}_A is the mean available fetch and F_E is the efficient fetch. F_{FAS} is calculated from Eq. 3.7. Fetches denoted with an asterisk (*) are limited by the surrounding shores of the Baltic.

	ØLANDS SÖDRA GRUND					HOBURG				
	\bar{F}_A	U_{10}^2	F_{FAS}	F_{FAS}/\bar{F}_A	F_E	\bar{F}_A	U_{10}^2	F_{FAS}	F_{FAS}/\bar{F}_A	F_E
Dir.	km	m^2/s^2	km	%	km	km	m^2/s^2	km	%	km
N	75	65.0	174	232	75*	60	70.9	190	315	60*
NE	185	77.4	207	112	185*	10	54.5	145	1450	10*
E	280	74.1	200	71	200	145	56.8	150	105	145*
SE	230	72.8	195	85	195	240	64.1	173	72	173
S	175	72.9	195	85	175*	250	65.2	173	70	175
SW	170	109.	290	172	170*	230	83.3	225	97	225
W	85	106.	285	334	85*	75	78.7	210	280	75*
NW	25	69.1	185	741	25*	85	63.5	170	200	85*

The fetches that are used in the wave generation by the mean wind speed are called the efficient fetches and are calculated in Table 4.2 and graphed in Figure 4.4.

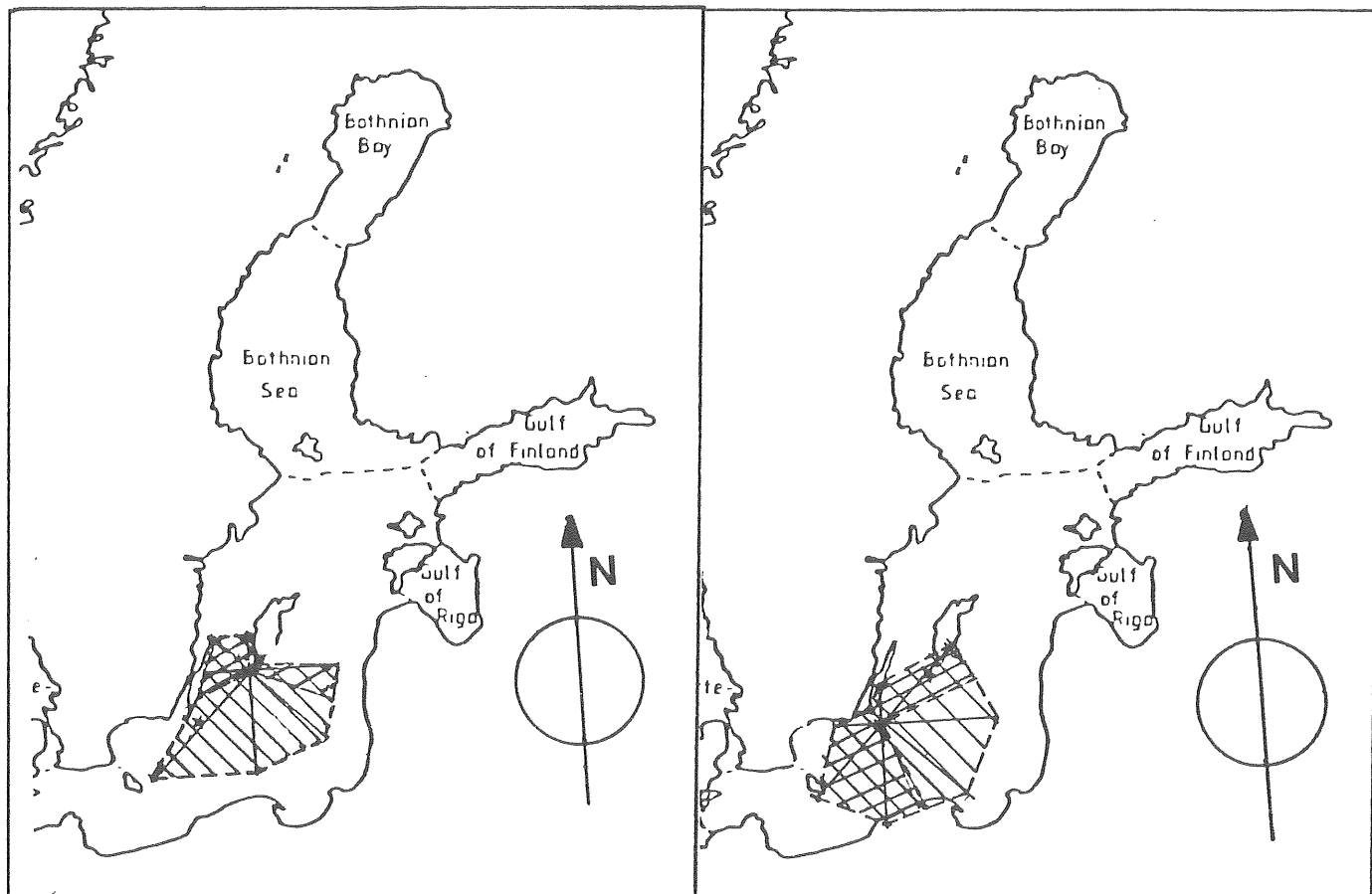


Figure 4.4a Mean efficient fetch for the wave generation at Hoburg.

Figure 4.4b Mean efficient fetch for the wave generation at Ølands södra grund.

In both figures the cross lined area is fetch limited, and the rest is for a FAS, as in Table 4.2.

As can be seen in Figure 4.4a the fetches in southerly directions are not limited for Hoburg. The unlimited fetches for ØSG is in the easterly to south-easterly directions. The efficient fetch area is larger for ØSG in prevailing wind directions.

This larger efficient fetch area together with the greater wind energy flux indicates that there should be more wave energy at ØSG. This is discussed in the following chapters (4.3-4.6), which are dealing with the wave measurings.

4.3 Wave climate evaluation

4.3.1 General aspects

In June 1981 a wave rider buoy was placed outside Hoburg, and then there were two wave measuring sites in the southern Baltic. This made it possible to evaluate the wave energy distribution somewhat and not just discuss it from the wind point of view.

As can be seen in Figure 4.5 for ØSG, there are two main directions of wave energy flux; east to south-west and north. Hoburg's main directions of wave energy flux are from south-west to south and east.

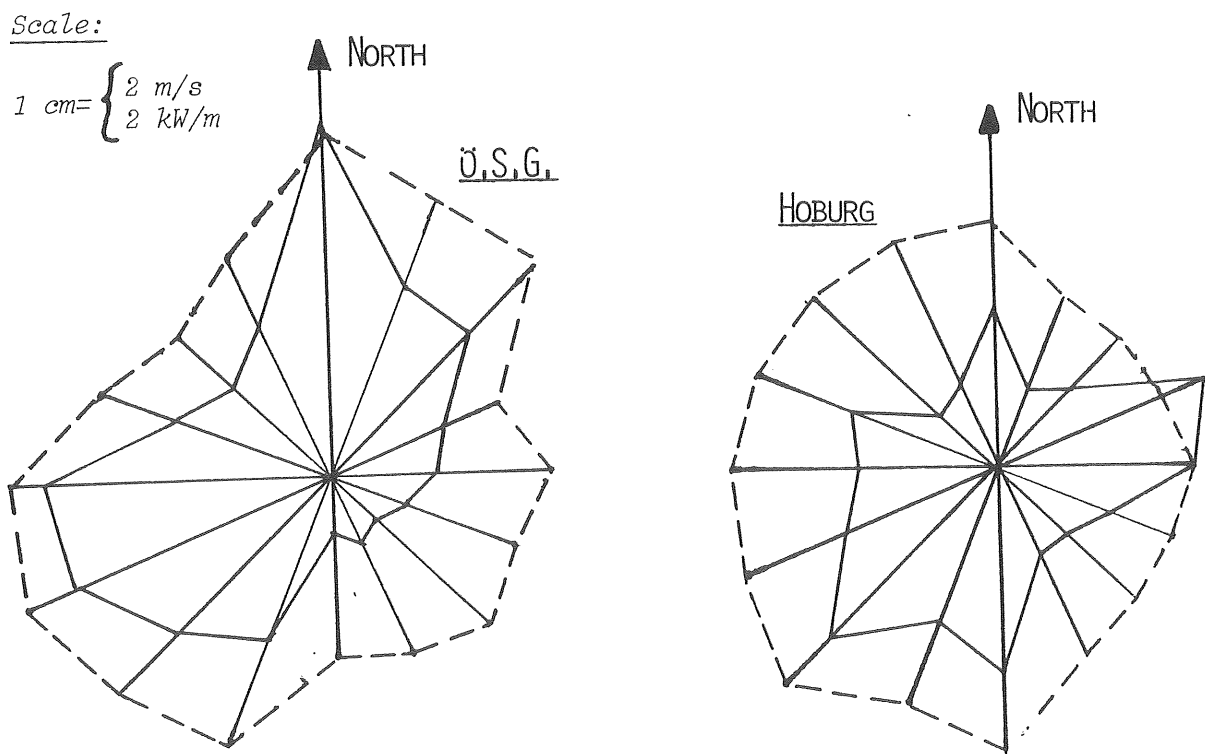


Figure 4.5 Directional distribution of the average wind speed (dashed line) and average wave power (solid line).

In the following, when discussing measured waves, the period of time referred to is from July 1, 1981 to January 23, 1982. This is 207 days. The waves are sampled in a time series, with an equidistant time of three hours, which makes eight data a day and a total of 1656 samples for each site.

The wave energy flux, P was approximately calculated using Eq. (3.9) as

$$P = 0.5 H_s^2 T_z \text{ (kW/m)} \quad (4.7)$$

where

H_s is the significant waveheight and
 T_z is the zero upcrossing period.

This gives a big difference in the mean wave power at the two sites. The mean wave powers are at

ØSG: $P = 5.1 \text{ kW/m}$

Hoburg: $P = 3.8 \text{ kW/m}$

Thus there is about 30% more wave energy at ØSG than at Hoburg.

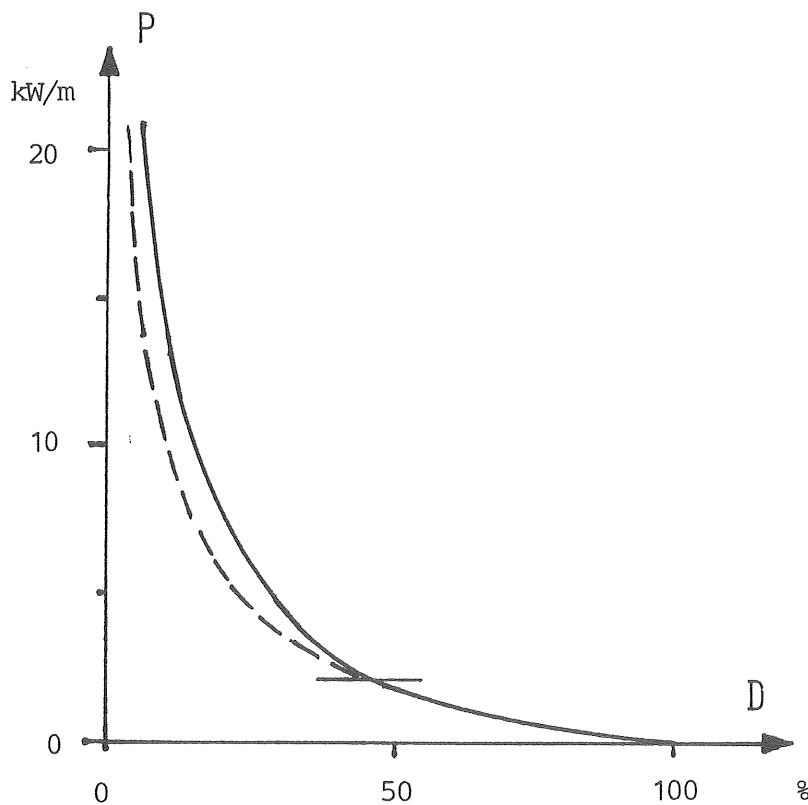


Figure 4.6 Wave power, P versus its frequency of exceedance, during the 207 days of measurements.

(ØSG - solid line, Hoburg - dashed line)

There is more wave energy at ØSG for wave powers greater than 2 kW/m, as can be seen in Figure 4.6.

Most of the energy is in the power range from 2 kW/m to 10 kW/m. Wave powers for ØSG are more frequent in that range and therefore the mean wave energy is greater.

The fluctuations of the wave power and the wind speed and direction are presented in Figure 4.7a (folded page). It is obvious that the wave power fluctuates quite rapidly. In ten hours the wave power can increase from zero up to 10 kW/m.

Due to fetch limitations, there sometimes are great differences in the wave power at the two sites even when the wind speed is equal. This occurs at the periods;

August 28-29, week 8, northerly winds
 November 4-9, week 18, northerly winds
 December 2, week 22, north-westerly wind
 December 18, week 24, north-westerly winds.

Note that ØSG has a shorter fetch in the norht-westerly direction and Hoburg in the northern direction, as can be seen in Table 4.2. Difference due to isobaric curvature are discussed in Chapter 4.4.

Fluctuations in the monthly average of wave power are considerable over the period and it varies from 2 kW/m to 15 kW/m. The mean wind speed varies between 5 m/s and 10 m/s.

Extreme values for the shown period is at

$$\begin{array}{ll} \text{ØSG: } \hat{\bar{P}} = 171 \text{ kW/m} & \hat{\bar{U}}_{10} = 23.9 \text{ m/s} \\ \text{Hoburg: } \hat{\bar{P}} = 63 \text{ kW/m} & \hat{\bar{U}}_{10} = 21 \text{ m/s} \end{array}$$

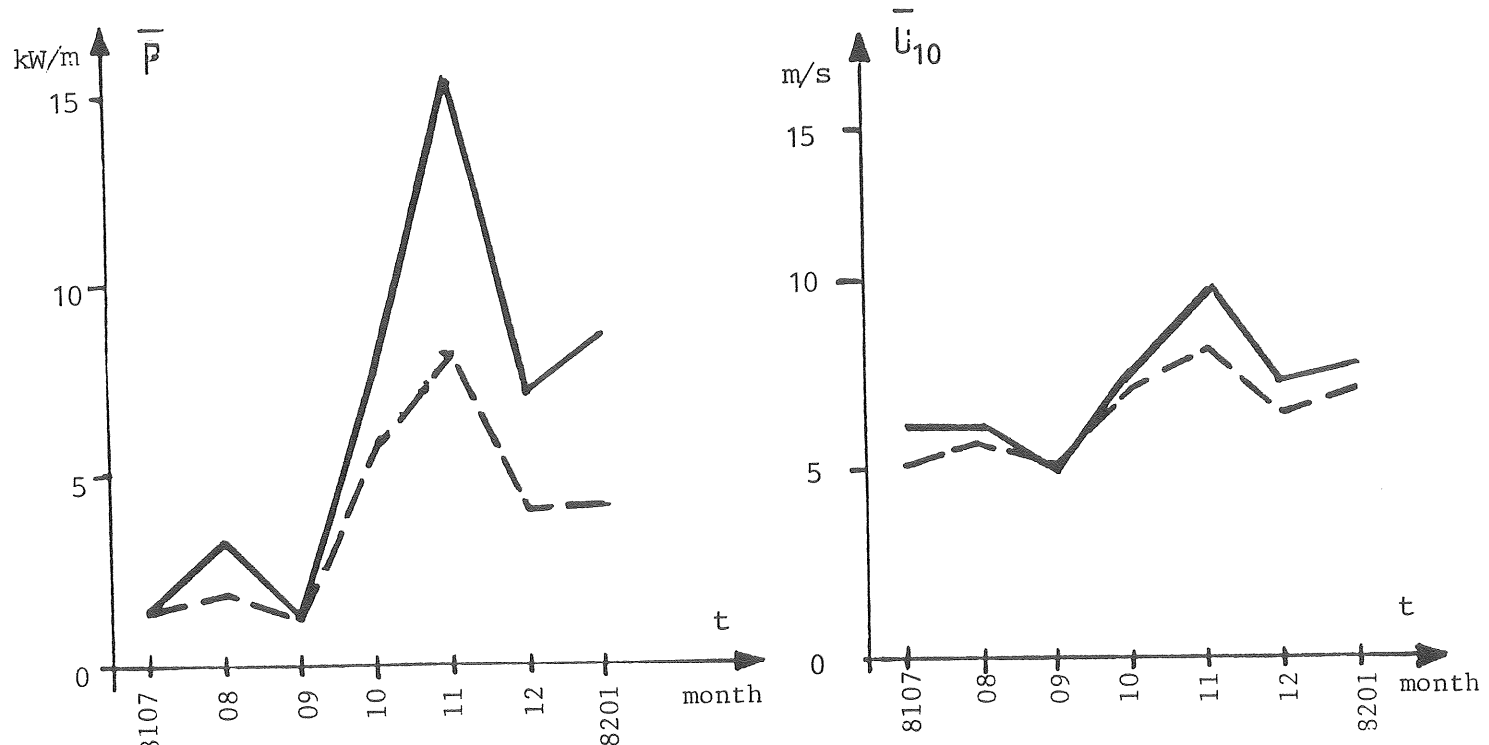


Figure 4.7b Monthly averaged wave power, \bar{P} and wind speed, \bar{U}_{10} .
(ØSG - solid line, Hoburg - dashed line)

4.3.2 Extreme month

November 1981 is a month of great interest. During November there were severe storms all over northern Europe, causing great damages. Due to rise of the sea level large areas were flooded by sea water.

During November the highest waves ever recorded in Swedish water occurred at ØSG. The maximum values of H_s was at

$$\text{ØSG: } \hat{H}_s = 6.2 \text{ m}$$

$$\text{Hoburg: } \hat{H}_s = 4.1 \text{ m}$$

both recorded the night between November 24 and 25. The measured zero upcrossing periods for these occasions were about $T_z = 13 \text{ s}$. The wind direction was from west.

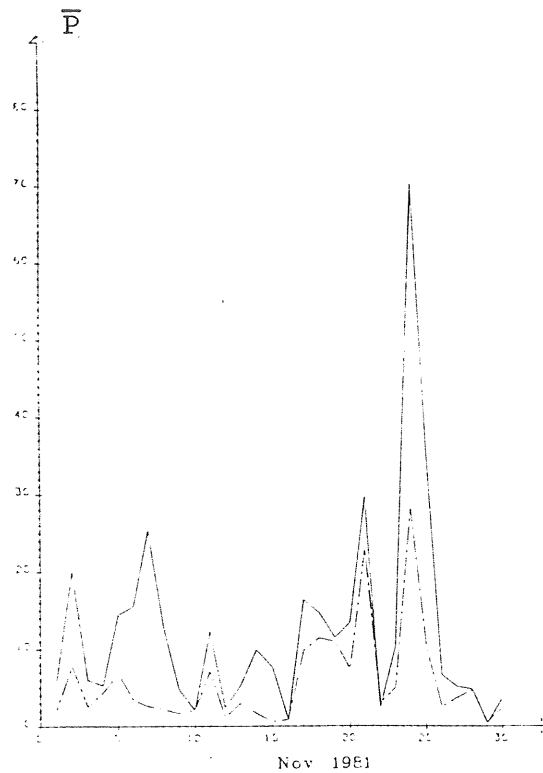


Figure 4.8 Daily averaged wave energy flux (\bar{P}) at ØSG and Hoburg in November 1981.
(ØSG - solid, Hoburg - dashed)

In Figure 4.9 directional generalized scatterdiagrams are presented. The generalization distinguishes which fetch directions that creates certain sea states.

During this month, November 1981, there were higher and longer waves at ØSG than at Hoburg, and obviously winds from west and south generated the high waves.

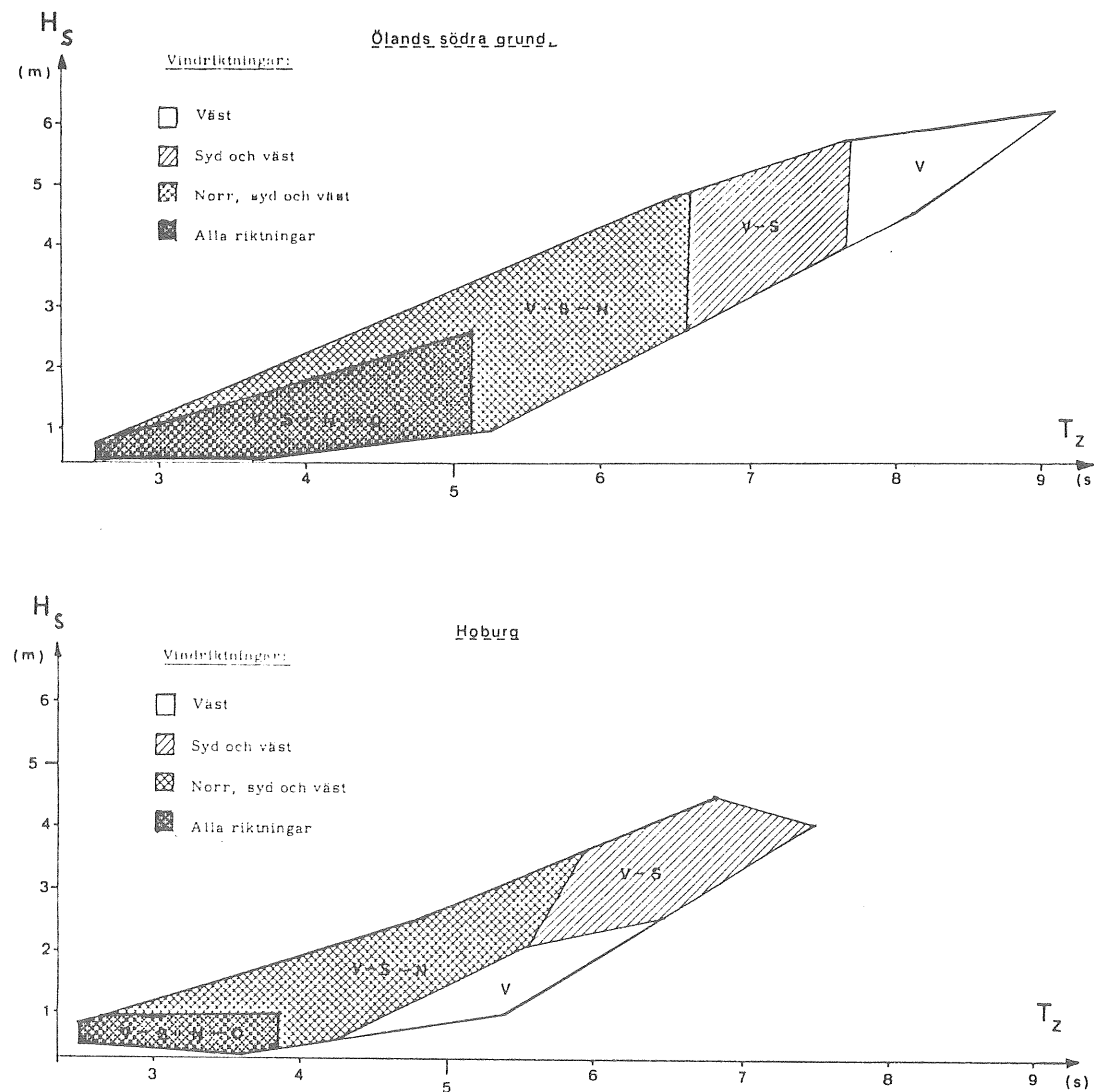


Figure 4.9 Directional generalization of the scatterdiagrams of November 1981, for ÖSG and Hoburg. (Direction translation: Norr-North, Syd-South, Väst-West, and "alla riktningar" - all direction.)

4.3.3 Wave parameters and scatterdiagrams

It is convenient to define the sea state at the two sites as probability distributions of the wave parameters H_s and T_z . A comparison is made in the figures below. (The step in T_z is 0.4 s and in H_s it is 0.8 m.)

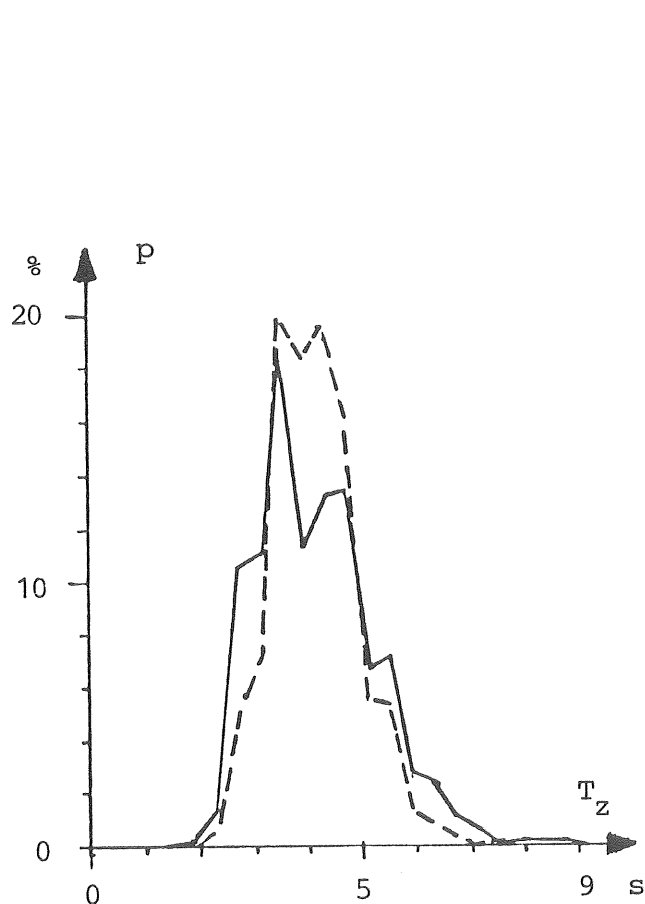


Figure 4.10a Probability distribution of T_z .

(ØSG - Solid line, Hoburg - dashed line.)

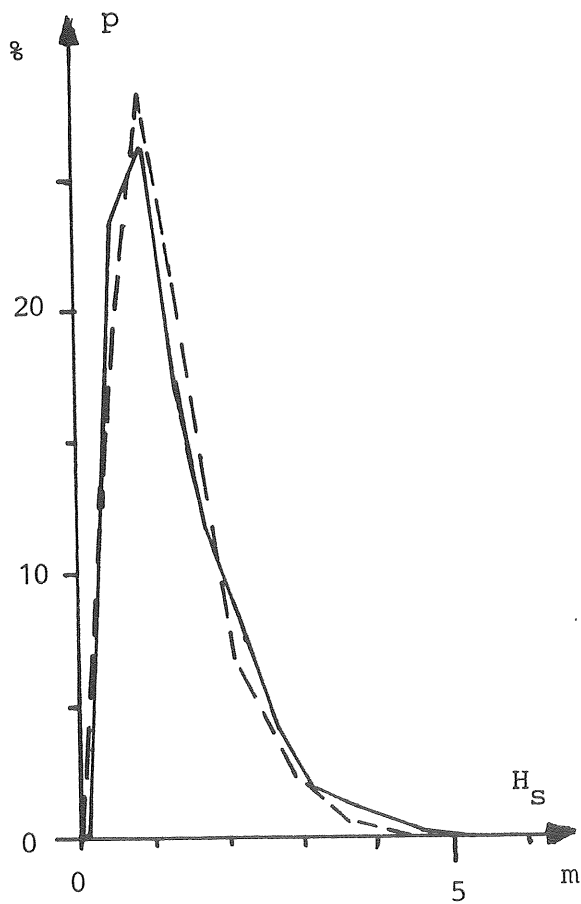


Figure 4.10b Probability distribution of H_s .

The probability distributions for the two measuring sites are quite equal, especially for H_s . Average values of H_s and T_z are nevertheless greater at ØSG than at Hoburg. With the use of scatter diagrams the correlation between H_s and T_z can be regarded.

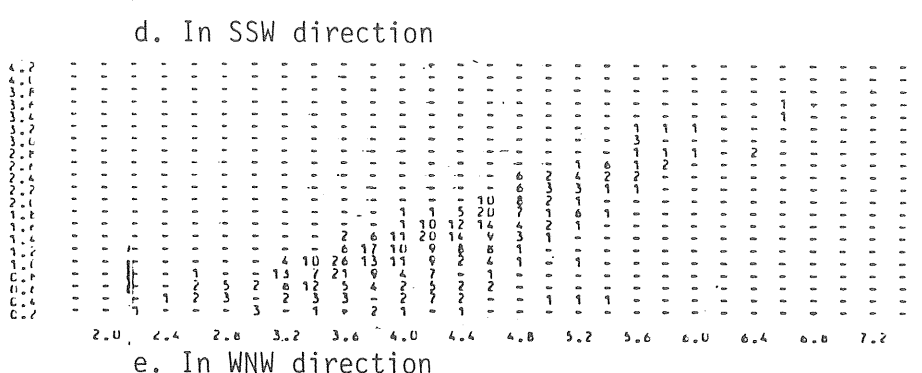
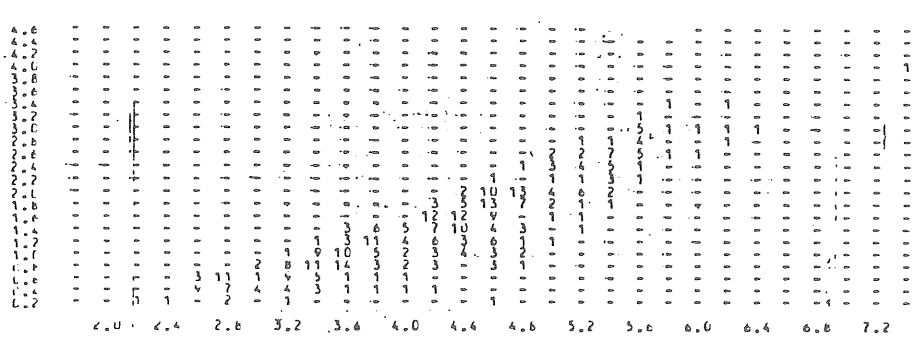
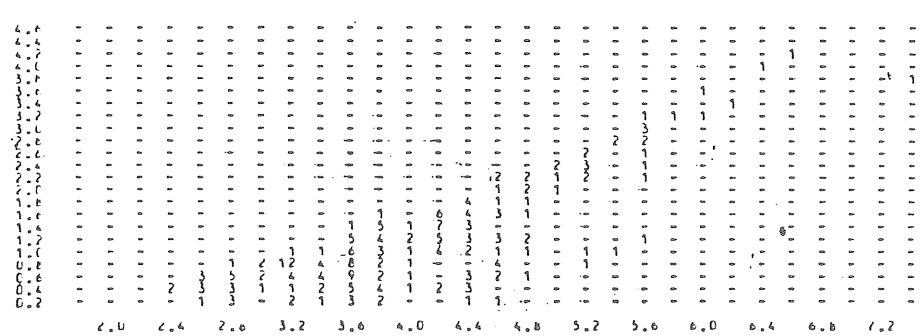
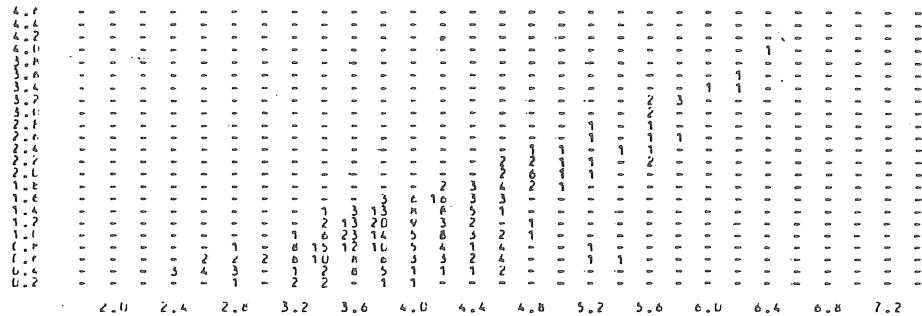
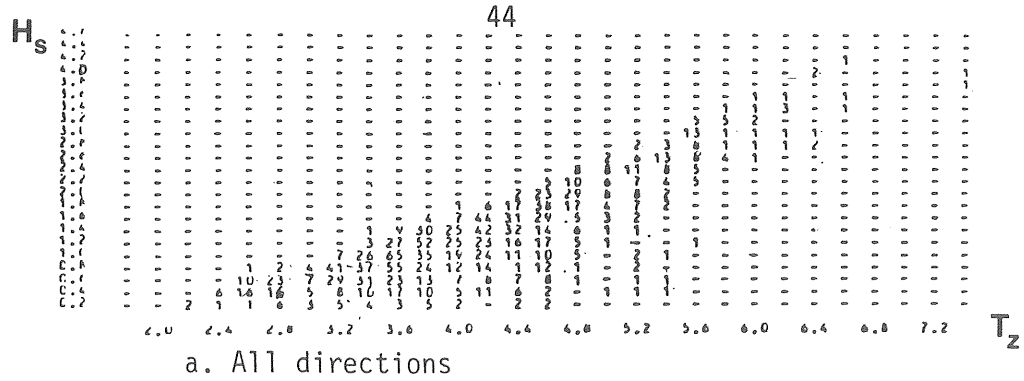


Figure 4.11 Scatter diagrams for Hoburg.

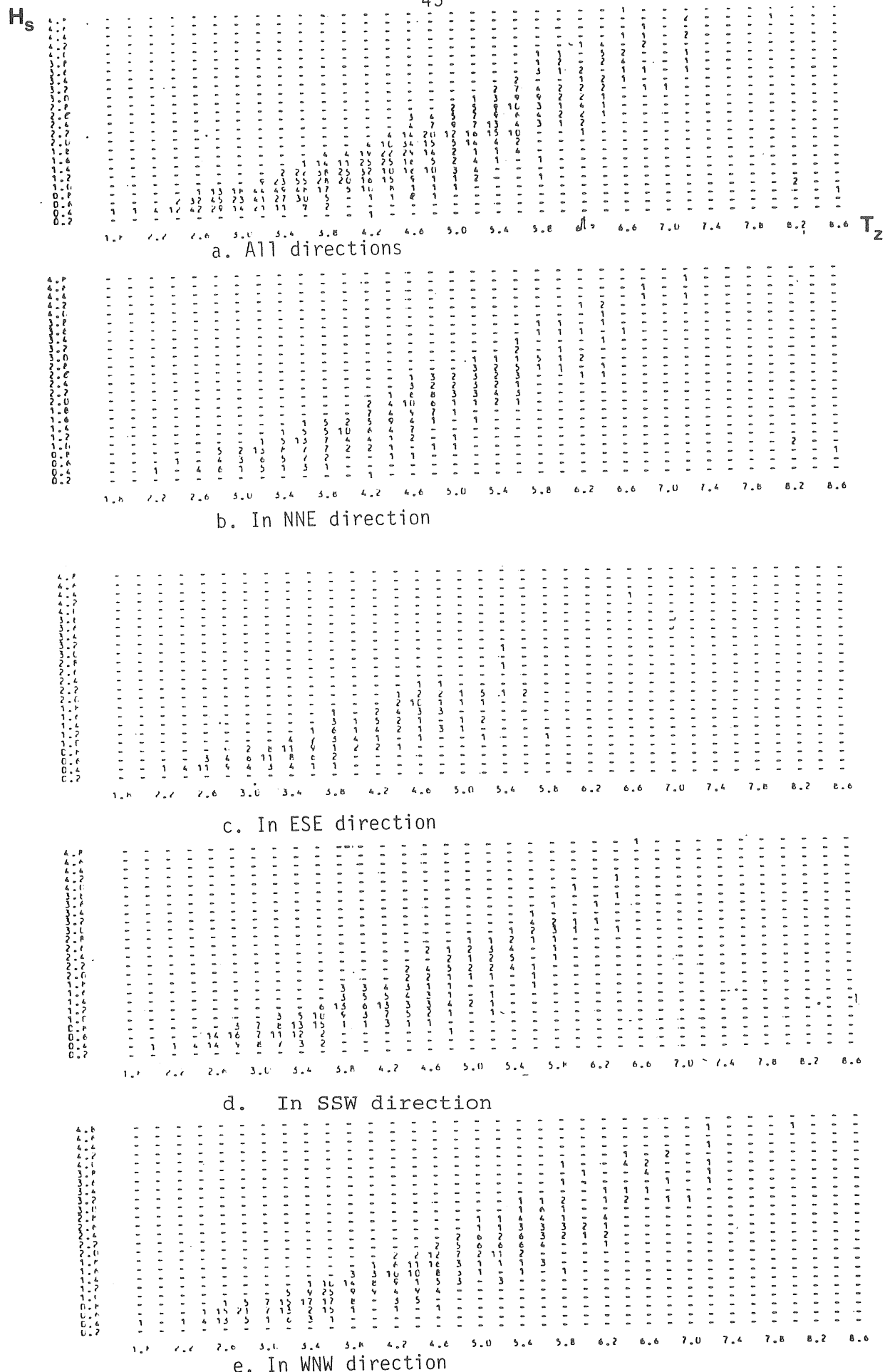


Figure 4.12 Scatter diagrams for ØSG.

Using the method of least squares and assuming that the significant wave height H_s is proportional to T_z^2 , it is possible to derive the most probable relation between H_s and T_z as follows.

The function is

$$H_s = C T_z^2 \quad (4.8)$$

where C is the regression-coefficient. C is derived by fitting the function Eq (4.8) to the scattered values in the sense of the least square method, which give the least variance, as is

$$C = \frac{\sum H_{s,i}}{\sum T_{z,i}^2} \quad (4.9)$$

The correlation between H_s and T_z^2 is expressed with the correlation coefficient, and it is

$$R = \frac{\mu_{TH}}{\sigma_T \sigma_H} \quad (4.10)$$

where σ^2 and μ are the variance and covariance between the regressed line and the scattered points. These functions are defined as follows

$$\sigma_T^2 = \frac{1}{N} \sum_{i=1}^n T_{z,i}^4 \quad (4.11)$$

$$\sigma_H^2 = \frac{1}{N} \sum_{i=1}^n H_{s,i}^4 \quad (4.12)$$

and

$$\mu_{TH} = C \cdot \sigma_T^2 \quad (4.13)$$

If H_s and T_z^2 are perfectly correlated then

$$R^2 = 1 \quad (4.14a)$$

and if there is no correlation

$$R = 0 \quad (4.14b)$$

The analyzed results show a better correlation, between H_s and T_z^2 , for ØSG than for Hoburg. In Table 4.3 the results of the regression analysis are shown.

Table 4.3 Regression results.

Location	Regr.coeff.	Corr.coeff.	Numbers
	C	R	N
ØSG	0.074	0.83	1526
Hoburg	0.073	0.73	1524
ØSG + Hoburg	0.073	0.79	3050

These derived relations can be of interest when discussing long term characteristics of the wave climate at the locations. Finally, the regression curves for the two locations are almost equal, why one can expect similar wave generation conditions.

It shall be noticed that the regression curves do not specify where the scattered values are placed along the curve.

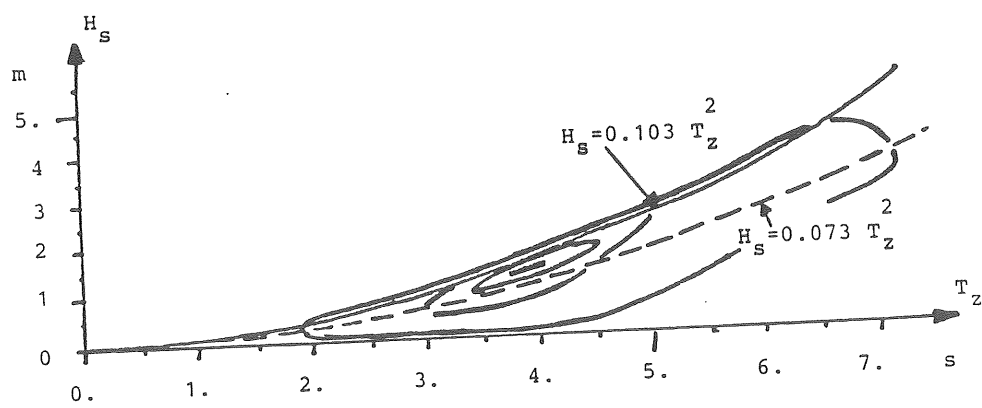


Figure 4.13 Summarized scatterdiagram for Hoburg and Ølands södra grund, schematically. The solid curve is the upper limit for a PM-spectrum, and the dotted curve is the most probable relation between H_s and T_z for the scattered values.

The maximum of C is obtained in a fully arisen sea (FAS) condition. With the use of a PM-spectrum it is specified to be $C=0.103$. This function is plotted as a solid line in Figure 4.13.

Comparing the results of the regression analysis with equivalently analyzed scatter diagrams from Utsira off Stavanger indicates that ØSG and Hoburg have a larger amount of more developed sea. (Station Utsira's regression coefficient $C=0.053$.)

4.4 Curvature of isobars

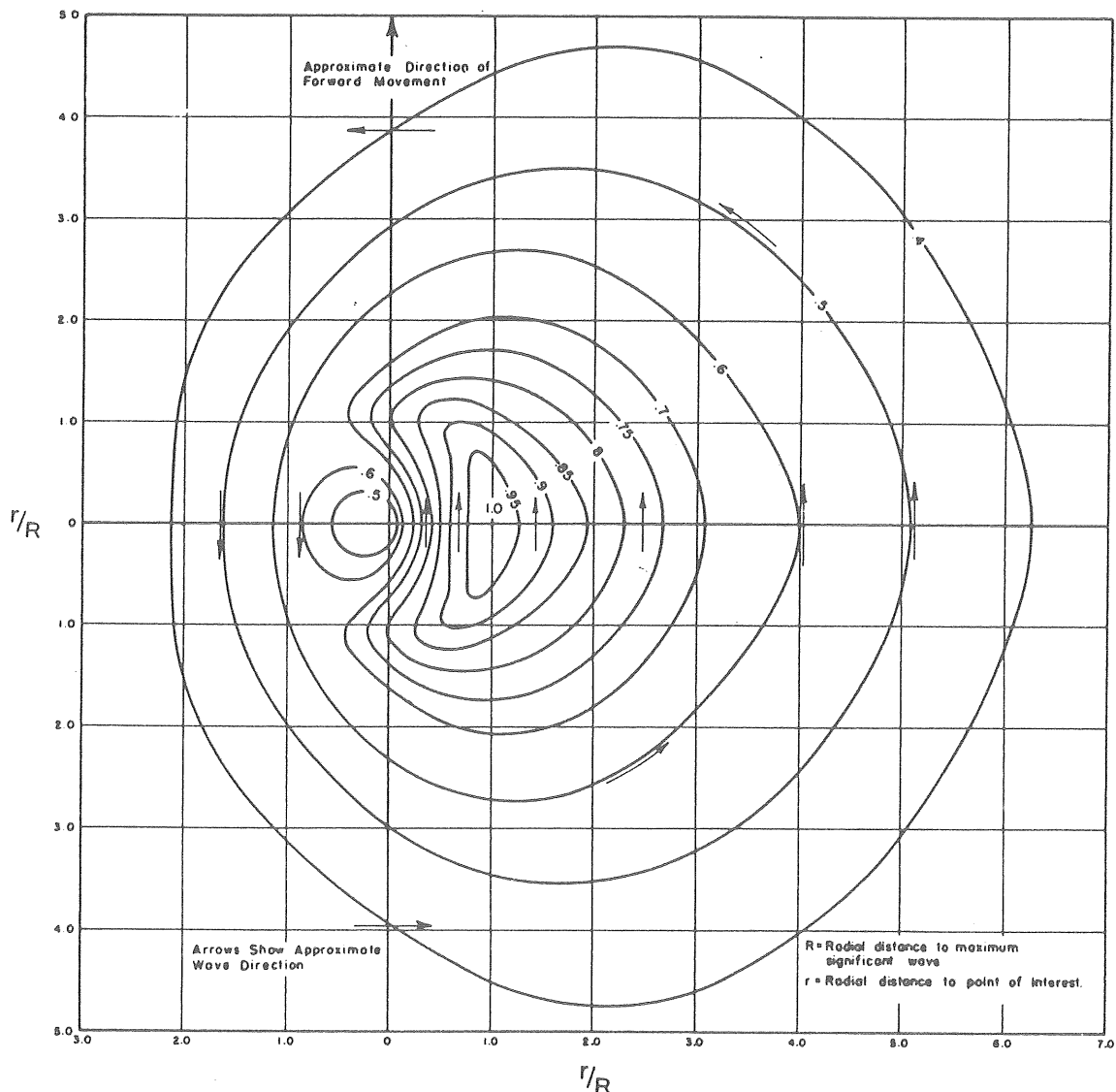


Figure 4.14 Isolines of relative significant wave height for slow-moving hurricane. (From Shore Protection Manual (1984))

Differences in the mean wind and in the geographical fetches have already been discussed. Viewing the wave energy time series (Figure 4.7), there are some situations when it is hard to explain the differences between the two sites. These situations have equivalent and high wind speeds but big differences in wave energy flux.

Apart from the coastline limitations there is one main source of inaccuracy. It is the curvature of the isobars. This is an important parameter when the wind speed exceeds 10-15 m/s at the measuring sites.

4.4.1 Theoretic wind speeds

At high wind speeds the wind to be analyzed cannot be regarded as geostrophic. Instead the gradient wind should be used. (Mårtensson (1983))

The gradient wind speed can be calculated as

$$U_{gr} = U_{gs} \pm \frac{U^2}{rf} \quad (4.15)$$

Here U_{gs} is the geostrophic wind

$$U_{gs} = \frac{1}{\rho f_c} \frac{\partial p}{\partial n} \quad (4.16)$$

$\partial p / \partial n$ is the horizontal pressure gradient perpendicular to the isobars

ρ is the density of the air; $\approx 1.25 \text{ kg/m}^3$

f_c is the Coriolis parameter; $= 1.454 \cdot 10^{-4} \sin \theta \text{ rad/s}$

where θ is the latitude

r is the radius of the isobars.

The minus sign in Eq. (4.15) is used for cyclones (low pressures) and the plus sign is used for anticyclones. Note that for straight isobars the wind is geostrophic.

Solving Eq. (4.15) for a low pressure gives with Eq. (4.16)

$$U_{gr} = -\frac{1}{2} rf_c + ((\frac{1}{2} rf_c)^2 + \frac{\Delta p}{\rho})^{\frac{1}{2}} \quad (4.18)$$

where Δp is the pressure difference between a point at the distance r from the lowpressure centre and the pressure in the centre.

The gradient wind is proportional to both the radius and the pressure difference.

4.4.2 Isobaric fetch limitations

A typical length scale of the fetches available at the two sites is 200 kilometres. If the isobars are considered to be circular, a deviation of more than 45 degrees from the average fetch direction will give a critical radius of 300 kilometres.

Using these assumptions in Eq. (4.18) gives the gradient wind

$$U_{gr} < -21.8 + (476 + 0.8 \Delta p)^{\frac{1}{2}} \quad (4.19)$$

The inequality is plotted in Figure 4.15 below.

In Figure 4.15 any measured quantity $(U_{gr}, \Delta p)$, that is below the curve, can have a limited fetch due to the curvature of the isobars.

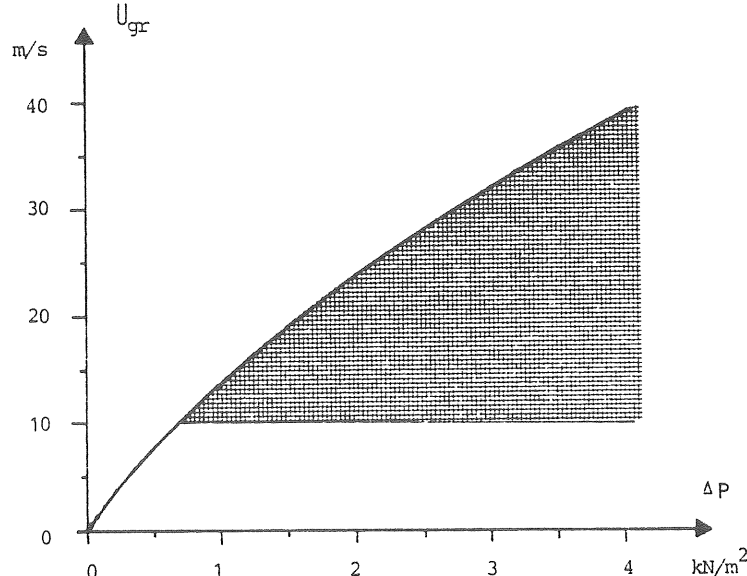


Figure 4.15 The gradient wind speed versus the pressure difference to the low pressure centre, assuming a critical radius of 300 kilometres. In the cross-lined area, fetch limitations due to isobaric curvature are to be expected.

Examining synoptic charts from the later part of 1981 gives that the wind speed must be greater than 10-15 m/s before there will be any significant curvature of the isobars. Furthermore they show an extremely good agreement between calculated (from air pressure) and measured wind speeds, when there are more or less circular isobars.

These two restrictions ($U_{gr} > 10$ m/s and Eq. 4.19) on U_{gr} and Δp combine into an area where fetch limitations due to isobaric curvature are to be expected. In Figure 4.15 this is the cross-lined area.

There are other reasons why isobars can curve, the ones to be considered are

- cold and warm weather fronts and
- when more than one low pressure centre are of major influence.

But for high wind speeds Eq. (4.19) is a good estimation.

It should thus, according to the above reasons, be noted that when calculating extreme wave conditions from wind data the isobaric curvature must be considered.

4.5 Shoaling effects at ØSG

Effects that can be important, but have not been considered here, are

- shoaling
- focusing
- diffraction and reflection from the lighthouse.

We will here explain why the shoaling effects can be neglected.

The measuring site at ØSG is located on a submarine ridge at a depth of 23 metres. Obviously the measured waves should be deformed due to shoaling.

Using linear wave theory it is possible to evaluate the error in the measured wave energy compared with that outside the submarine ridge.

Because of the conservation of energy, a wave travelling from infinite depth into water at finite depth will change in height from H_0 to H . The governing equation is

$$H = K_s H_0 \quad (4.20)$$

with

$$K_s = \left(\frac{k_0}{k} \left(1 + \frac{2 kd}{\sinh 2kd} \right) \right)^{-\frac{1}{2}} \quad (4.21)$$

Here

$k = 2\pi/L$ is the wave number

L = the wave length

d = the water depth.

The wave length is changing while travelling into shallower water.

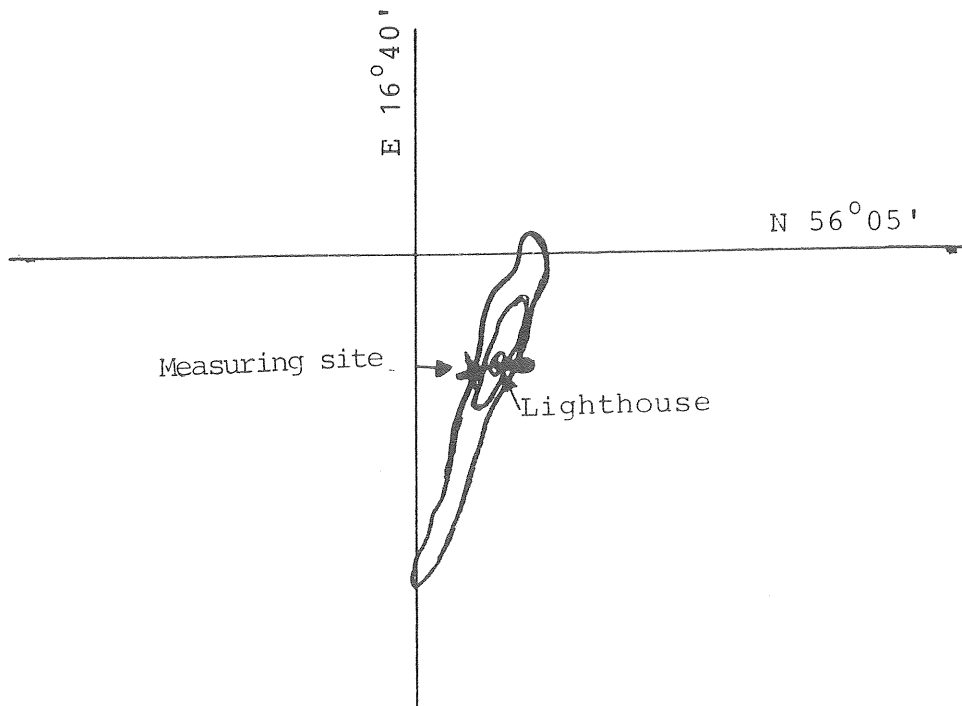


Figure 4.16 Bottom contours of Ølands södra grund (ØSG). Outer contour at 20 m, and the rest with an equidistance of 5 metres. (Scale 1:1000000)

The two parameters, wave number and angular frequency ($\omega=2\pi f$), are dispersively related as

$$\omega^2 = gk \tanh(kd) \quad (4.22)$$

Assuming that the wave height is twice the amplitude it is possible to derive the change in energy content in the waves. This is shown in Figure 4.16 for three various depths. These depths are representative for:

$d = 45$ m: depth of the surrounding ocean

$d = 23$ m: depth of the measuring site

$d = 14$ m: depth at the shallowest part of the ridge.

When comparing with infinite depth, the error in the estimated wave energy is

$$\Delta E = \frac{1}{28} \sum_{i=4}^{31} \frac{\frac{a_i^2}{2}}{\frac{a_{oi}^2}{2}} = 0.03 \quad (4.23)$$

which is of the same scale as other errors in the analysis, and is therefore neglected.

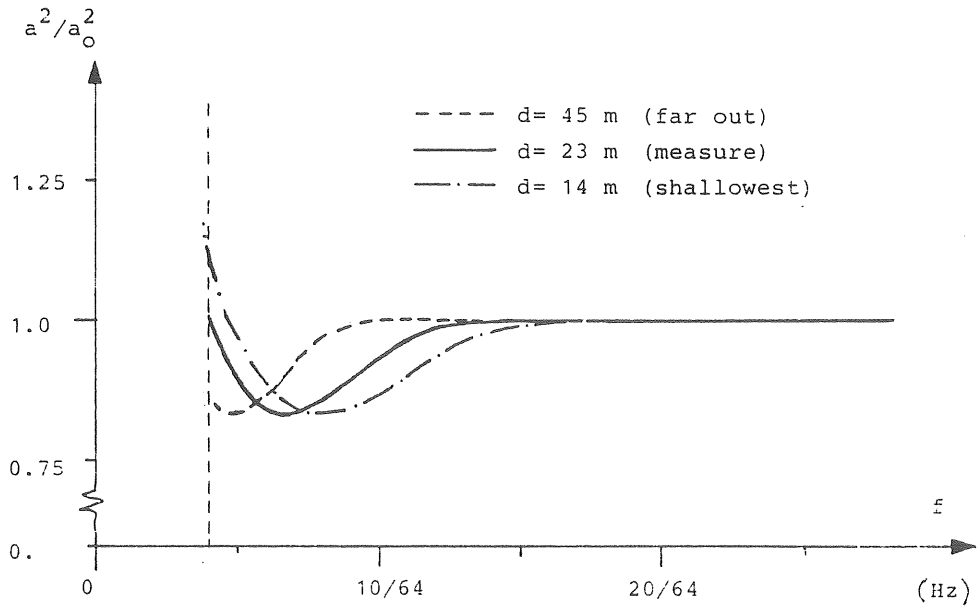


Figure 4.17 Normalized wave energy (to deep water energy) versus frequency. The frequency is discretized between 4 and 31 times the frequency step ($1/64$ Hz), as from Chapter 2.

The surrounding ocean has an average depth of 45 metres, shoaling effects at the measuring site should therefore be compared with this depth. This gives an error that is even smaller, $\Delta E=0.005$.

Errors due to wave breaking, while passing the shallowest part of the ridge, are neglected. This occurs for easterly waves.

LIST OF ABBREVIATIONS AND SYMBOLS

Abbreviations

AM	Amplitude Modulated
EFN	Swedish Energy Research Commission
FAS	Fully Arisen Sea
FFT	Fast Fourier Transform
JONSWAP	Joint North Sea Wave Project
NS	North Sea
PM	Pierson-Moskowitz
SMHI	Swedish Meteorological and Hydrological Institute
ØSG	Ølands södra grund (Shoal south of the island of Øland)

Symbols

A	Regression coefficient between wave energy flux and the product of H_s squared and T_z .
a	Wave amplitude
a_0	Wave amplitude at infinite water depth
C	Regression coefficient between H_s and T_z squared
d	Water depth
E	Wave energy
F	Fetch
F_A	Available fetch (geographically)
F_E	Efficient fetch, i.e. the actually used fetch in wave generation
F_{FAS}	Fetch required for a FAS
F_0	Normalized fetch

f	Wave frequency
f_c	Coriolis parameter
g	Acceleration of gravity
H	Wave height
H_s	Significant wave height
H_o	Wave height at infinite water depth
H_{10}	The tenth highest wave
K_s	Shoaling coefficient
k	Wave number
k_o	Wave number at infinite water depth
m_o	Wave spectral moment of zeroth order
m_2	Wave spectral moment of second order
N	Number of waves, occurrence etc.
n	Normal direction
P	Wave energy flux
P_w	Wind energy flux
\bar{P}_{79}	Mean wave energy flux in 1979
\bar{P}_{80}	Mean wave energy flux in 1980
p	Probability of occurrence
p	Air pressure

R	Correlation coefficient
r	Radial distance to low pressure centre
S	Wave spectral density
T	Wave period
T_z	Wave zero-upcrossing period
U	Wind speed
U_{gr}	Gradient wind speed
U_{gs}	Geostrophic wind speed
U_{10}	Wind speed at 10 metres height above the surface
α	Phillips constant (for a wave spectrum)
α_{FAS}	Phillips constant for FAS
Δ	Increment of variable
∂	Infinitesimal increment
Θ	Latitude
μ	Mean value
ρ	Density of either water or air
σ	Standard deviation
ω	Wave angular frequency
$\hat{-}$	Extreme value
$\bar{-}$	Average value

LIST OF FIGURES

- Figure 1.1 Wave measurements are carried out (with fixed devices at the three lighthouses Almagrundet, Ölands södra grund and Trubaduren, and with a mobile device at Hoburg and Väderöarna.
- Figure 2.1 The inverted echo-sounder is placed on the sea bed at a depth of 25 m and about 100 m from the lighthouse. (From Mattisson (1980))
- Figure 2.2 Generalized flow chart of the microprocessor program. (Mattisson (1980))
- Figure 3.1 Mean energy flux. The dashed line is from the obtained (measured) series, and the solid line from the created series.
- Figure 3.2 Scatterdiagrams for all wind directions.
- Figure 3.3a Scatterdiagram (1979) for wind direction N and NE
- Figure 3.3b Scatterdiagram (1979) for wind direction E and SE
- Figure 3.3c Scatterdiagram (1979) for wind direction S and SW
- Figure 3.3d Scatterdiagram (1979) for wind direction W and NW
- Figure 3.4a Scatterdiagram (1980) for wind direction N and NE
- Figure 3.4b Scatterdiagram (1980) for wind direction E and SE
- Figure 3.4c Scatterdiagram (1980) for wind direction S and SW
- Figure 3.4d Scatterdiagram (1980) for wind direction W and NW
- Figure 3.5a Scatterdiagram (1979-1980) for wind direction N and NE
- Figure 3.5b Scatterdiagram (1979-1980) for wind direction E and SE
- Figure 3.5c Scatterdiagram (1979-1980) for wind direction S and SW
- Figure 3.5d Scatterdiagram (1979-1980) for wind direction W and NW
- Figure 3.6 Wave energy flux versus probability of occurrence. The solid line is the average and the dashed lines are minimum and maximum. (Wave data from Ø.S.G.)
- Figure 3.7 Accumulated energy distribution versus propagation direction and frequency (mean of the eighth cardinal direction). The distributions are for the created years.
- Figure 4.1 Measuring sites in the southern Baltic, at Ölands södra grund and Hoburg.

- Figure 4.2a The probability, p , of the occurrence of wind speeds, U .
- Figure 4.2b Cumulated probability versus wind speed.
- Figure 4.3 The directional distribution of the average wind velocity and the average wind energy flux, according to Table 4.1. (ØSG - solid line, Hoburg - dashed line)
- Figure 4.4a Mean efficient fetch for the wave generation at Hoburg.
- Figure 4.4b Mean efficient fetch for the wave generation at Ølands södra grund.
- Figure 4.5 Directional distribution of the average wind speed (dashed line) and average wave power (solid line).
- Figure 4.6 Wave power, P versus its frequency of exceedance, during the 207 days of measurements.
- Figure 4.7a Wave power, wind speed and direction versus time (in weeks from 1 July, 1981) (ØSG and Hoburg)
- Figure 4.7b Monthly averaged wave power, \bar{P} and wind speed, \bar{U}_{10} .
- Figure 4.8 Daily averages wave energy flux (\bar{P}) at ØSG and Hoburg in November 1981.
- Figure 4.9 Direktional generalization of the scatterdiagrams of November 1981, for ØSG and Hoburg. (Direction translation: Norr-North, Syd-South, Väst-West, and "alla riktningar" - all direction.)
- Figure 4.10a Probability distribution of T_z .
- Figure 4.10b Probability distribution of H_s .
- Figure 4.11 Scatter diagrams for Hoburg.
 - All directions.
 - In NNE direction.
 - In ESE direction.
 - In SSW direction.
 - In WNW direction.
- Figure 4.12 Scatter diagrams for ØSG.
 - All directions.
 - In NNE direction.
 - In ESE direction.
 - In SSW direction.
 - In WNW direction.
- Figure 4.13 Summarized scatterdiagram for Hoburg and Ølands södra grund, schematically. The solid curve is the upper limit for a PM-spectrum, and the dotted curve is the most probable relation between H_s and T_z for the scattered values.

Figure 4.14 Isolines of relative significant wave height for slow-moving hurricane. (From Shore Protection Manual (1984))

Figure 4.15 The gradient wind speed versus the pressure difference to the low pressure centre, assuming a critical radius of 300 kilometres. In the cross-lined area, fetch limitations due to isobaric curvature are to be expected.

Figure 4.16 Bottom contours of Ölands södra grund (ÖSG). Outer contour at 20 m, and the rest with an equidistance of 5 metres. (Scale 1:1000000)

Figure 4.17 Normalized wave energy (to deep water energy) versus frequency. The frequency is discretized between 4 and 31 times the frequency step (1/64 Hz), as from Chapter 2.

REFERENCES

Gran, Sverre (1977): Estimates of wave power at the coast of Norway. Techn.rep.no. 77-570, Det norske Veritas, Høvik, Norway.

Hasselman et al (1973): Measurements of Wind-Wave Growth and Swell Decay during the Joint North Sea Wave Project (JONSWAP). Erg.-heft z- Deutsches Hydrgr. Zeischrift, Reihe A(8⁰), Nr 12, Deuts.Hydrogr. Inst., Hamburg, Germany.

Mattison, Ingemar (1980): A wave measuring project for wave energy prospecting purpose. Proc. "Seminarium om vågdata för vågenergi Trondheim 1-3 December 1980", Gr. Vågenergifo., Rap.Gr:36 (1981), Trondheim/Göteborg, Norw./Sweden.

Mårtensson, Nils (1983): Wind Generated Waves. Gr. Wave energy research, Report GR:52, 2nd ed. Göteborg, Sweden (ISSN 0280-5987).

Rylander (1980): Hindcasting calculations. (unpublished)

Shore Protection Manual (1984), Coastal Engineering Research Center, Department of the Army, Waterway's Experiment Station, Corps of Engineers, Vicksburg, Missouri, USA.

BIBLIOGRAPHY

Box, Hunter and Hunter (1978): Statistics for experimenters. John Wiley & Sons, New York, USA.

Houmb and Qwam (1979): A comparison of the wave climate at Utsira, Halten and Tromsøflaket based on duration of sea state. Inst. Havnebyggnning, Report no.10 1979, NTH, Trondheim, Norway.

Houmb and Øyan (1981): Fits between empirical spectra and the JONSWAP model. Div.Port and Ocean Eng., Report no.5 1981, NTH, Trondheim, Norway.

Håland and Småland (1980): Final Raport. Frequency tables of significant wave height and extreme values for selected positions at the continental shelf. Norwegian Meteorological Institute, Oslo/Bergen, Norway.

Karlsson, Torbjörn (1969): Refraction of continuous wave spectra. J.Waterways and Harbors Div., 95(1969), WW4. ASCE.

Krogstad, Harald (1979): Bølgeenergifluks mot fire målestasjoner utenfor Norskekysten. Inst.f.kontinentalsokkelsundersøkelser (IKU), Norway.

Kvick, Andersson och Fredriksson (1983): Vindarna över Sverige. (Projektresultat). Nämnden för energiproduktionsforskning NE, NE 1983:16, Stockholm, Sweden.

Norrbin, Nils (1966): Vågor, vågspektra och visuella vågdata. Publ. rep. SSPA Nr:17, Göteborg, Sweden.

Råde och Rudemo (1975); Sannolikhetslära och statistik för teknisk högskola. Del 1. Biblioteksförlaget, Stockholm, Sweden.

Svensson, J (1981): Vågdata från svenska kustvatten 1979-1980. Report RHO 30, SMHI, Norrköping, Sweden.

Svensson, Jonny (1982): Vågdata från svenska kustvatten 1981.
Report HB 53, SMHI, Norrköping, Sweden.

Sørensen and Frederiksen (1977): A preliminary review of waves on
the Danish North Sea coast as a source of energy. Danish
Hydraulic Institute (DHI), Denmark.

Wahl, Gösta (1973): Vågstatistik från svenska kustfarvatten -
fryskeppet Fladen. Publ. rep. SSPA Nr:35, Göteborg, Sweden.

Wahl, Gösta (1973): Vågstatistik från svenska kustfarvatten -
fryskeppet Svenska Björn. Publ. rep. The Swed. State Shipb.
and Exp. Tank, No:36, Göteborg, Sweden.

Wahl, Gösta (1973): Vågstatistik från svenska kustfarvatten -
fryskeppet Finngrundet. Publ. rep. SSPA Nr:37, Göteborg,
Sweden.

Wahl, Gösta (1973): Vågstatistik från svenska kustfarvatten -
fryskeppet Falsterborev. Publ. rep. SSPA Nr:38, Göteborg,
Sweden.

Wahl, Gösta (1974): Wave Statistics from Swedish Coastal Waters.
Proc. The dynamics of marine vehicles and structures in
waves, Paper no:4, London (1974-04-01 - 05), GB.

CHALMERS TEKNISKA HÖGSKOLA
Institutionen för vattenbyggnad

Report Series A

- A:1 Bergdahl, L.: Physics of ice and snow as affects thermal pressure. 1977.
- A:2 Bergdahl, L.: Thermal ice pressure in lake ice covers. 1978.
- A:3 Häggström, S.: Surface Discharge of Cooling Water. Effects of Distortion in Model Investigations. 1978.
- A:4 Sellgren, A.: Slurry Transportation of Ores and Industrial Minerals in a Vertical Pipe by Centrifugal Pumps. 1978.
- A:5 Arnell, V.: Description and Validation of the CTH-Urban Runoff Model. 1980.
- A:6 Sjöberg, A.: Calculation of Unsteady Flows in Regulated Rivers and Storm Sewer Systems. 1976.
- A:7 Svensson, T.: Water Exchange and Mixing in Fjords. Mathematical Models and Field Studies in the Byfjord. 1980.
- A:8 Arnell, V.: Rainfall Data for the Design of Sewer Pipe Systems. 1982.
- A:9 Lindahl, J., Sjöberg, A.: Dynamic Analysis of Mooring Cables. 1983.
- A:10 Nilsdal, J-A.: Optimeringsmodellen ILSD. Beräkning av topografins inverkan på ett dagvattensystems kapacitet och anläggningskostnad. 1983.
- A:11 Lindahl, J.: Implicit numerisk lösning av rörelseekvationerna för en förankringskabel. 1984.
- A:12 Lindahl, J.: Modellförsök med en förankringskabel. 1985.
- A:13 Lyngfelt, S.: On Urban Runoff Modelling. The Application of Numerical Models Based on the Kinematic Wave Theory. 1985.
- A:14 Johansson, M.: Transient Motions of Large Floating Structures. 1986.
- A:15 Mårtensson, N., Bergdahl, L.: On the Wave Climate of the Southern Baltic. 1987.

Report Series B

- B:1 Bergdahl, L.: Beräkning av vågkrafter. (Ersatts med 1979:07) 1977.
- B:2 Arnell, V.: Studier av amerikansk dagvattenteknik. 1977.
- B:3 Sellgren, A.: Hydraulic Hoisting of Crushed Ores. A feasibility study and pilot-plant investigation on coarse iron ore transportation by centrifugal pumps. 1977.
- B:4 Ringesten, B.: Energi ur havsströmmar. 1977.
- B:5 Sjöberg, A., Asp, T.: Brukar-anvisning för ROUTE-S. En matematisk modell för beräkning av icke-stationära flöden i floder och kanaler vid strömmande tillstånd. 1977.
- B:6 Annual Report 1976/77. 1977.
- B:7 Bergdahl, L., Wernersson, L.: Calculated and Expected Thermal Ice Pressures in Five Swedish Lakes. 1977.
- B:8 Göransson, C-G., Svensson, T.: Drogue Tracking - Measuring Principles and Data Handling. 1977.
- B:9 Göransson, C-G.: Mathematical Model of Sewage Discharge into confined, stratified Basins - Especially Fjords. 1977.
- B:10 Arnell, V., Lyngfelt, S.: Beräkning av dagvattenavrinning från urbana områden. 1978.
- B:11 Arnell, V.: Analysis of Rainfall Data for Use in Design of Storm Sewer Systems. 1978.
- B:12 Sjöberg, A.: On Models to be used in Sweden for Detailed Design and Analysis of Storm Drainage Systems. 1978.
- B:13 Lyngfelt, S.: An Analysis of Parameters in a Kinematic Wave Model of Overland Flow in Urban Areas. 1978.
- B:14 Sjöberg, A., Lundgren, J., Asp, T., Melin, H.: Manual för ILLUDAS (Version S2). Ett datorprogram för dimensionering och analys av dagvattensystem. 1979.
- B:15 Annual Report 1978/79. 1979.
- B:16 Nilsdal, J-A., Sjöberg, A.: Dimensionerande regn vid höga vattenstånd i Göta älv. 1979.
- B:17 Stöllman, L-E.: Närkes Svartå. Hydrologisk inventering. 1979.
- B:18 Svensson, T.: Tracer Measurements of Mixing in the Deep Water of a Small, Stratified Sill Fjord. 1979.
- B:19 Svensson, T., Degerman, E., Jansson, B., Westerlund, S.: Energiutvinning ur sjö- och havssediment. En förstudie. R76:1980. 1979.

- B:20 Annual Report 1979. 1980.
- B:21 Stöllman, L-E.: Närkes Svartå. Inventering av vatten-tillgång och vattenanvändning. 1980.
- B:22 Häggström, S., Sjöberg, A.: Effects of Distortion in Physical Models of Cooling Water Discharge. 1979.
- B:23 Sellgren, A.: A Model for Calculating the Pumping Cost of Industrial Slurries. 1981.
- B:24 Lindahl, J.: Rörelseekvationen för en kabel. 1981.
- B:25 Bergdahl, L., Olsson, G.: Konstruktioner i havet. Våg-krafter-rörelser. En inventering av datorprogram. 1981.
- B:26 Annual Report 1980. 1981.
- B:27 Nilsdal, J-A.: Teknisk-ekonomisk dimensionering av av-loppsledningar. En litteraturstudie aom datormodeller. 1981.
- B:28 Sjöberg, A.: The Sewer Network Models DAGVL-A and DAGVL-DIFF. 1981.
- B:29 Moberg, G.: Anläggningar för oljeutvinning till havs. Konstruktionstyper, dimensioneringskriterier och posi-tioneringssystem. 1981.
- B:30 Sjöberg, A., Bergdahl, L.: Förankringar och förankrings-krafter. 1981.
- B:31 Häggström, S., Melin, H.: Användning av simuleringsmo-dellen MITSIM vid vattenresursplanering för Svartån. 1982.
- B:32 Bydén, S., Nielsen, B.: Närkes Svartå. Vattenöversikt för Laxå kommun. 1982.
- B:33 Sjöberg, A.: On the stability of gradually varied flow in sewers. 1982.
- B:34 Bydén, S., Nyberg, E.: Närkes Svartå. Undersökning av grundvattenkvalitet i Laxå kommun. 1982.
- B:35 Sjöberg, A., Mårtensson, N.: Regnenveloppmetoden. En analys av metodens tillämpelighet för dimensionering av ett 2-års perkolationsmagasin. 1982.
- B:36 Svensson, T., Sörman, L-O.: Värmeupptagning med botten-förlagda kyrlslangar i stillastående vatten. Laboratorie-försök. 1982.
- B:37 Mattsson, A.: Koltransporter och kolhantering. Lagring i terminaler och hos storförbrukare. (Delrapport). 1983.
- B:38 Strandner, H.: Ett datorprogram för sammankoppling av ILLUDAS och DAGVL-DIFF. 1983.

- B:39 Svensson, T., Sörman, L-O.: Värmeupptagning med bottenförlagda slangar i rinnande vatten. Laboratorieförsök. 1983.
- B:40 Mattsson, A.: Koltransporter och kolhantering. Lagring i terminaler och hos storförbrukare. Kostnader. Delrapport 2. 1983.
- B:41 Häggström, S., Melin, H.: Närkes Svartå. Simuleringsmodellen MITSIM för kvantitativ analys i vattenresursplanering. 1983.
- B:42 Hård, S.: Seminarium om miljöeffekter vid naturvärmesystem. Dokumentation sammanställd av S. Hård, VIAK AB. BFR-R60:1984. 1983.
- B:43 Lindahl, J.: Manual för MODEX-MODIM. Ett datorprogram för simulerings av dynamiska förlopp i förankringskablar. 1983.
- B:44 Activity Report. 1984.
- B:45 Sjöberg, A.: DAGVL-DIFF. Beräkning av icke-stationära flödesförlopp i helt eller delvis fyllda avloppssystem, tunnlar och kanaler. 1984.
- B:46 Bergdahl, L., Melin, H.: WAVE FIELD. Manual till ett program för beräkning av ytvattenvågor. 1985.
- B:47 Lyngfelt, S.: Manual för dagvattenmodellen CURE. 1985.
- B:48 Perrusquia, G., Lyngfelt, S., Sjöberg, A.: Flödeskapacitet hos avloppsledningar delvis fyllda med sediment. En inledande experimentell och teoretisk studie. 1986.
- B:49 Bergdahl, L., Lindahl, J.: MODEX-MODIM. User's Manual. 1987.

